Evaluation of Global Ozone Monitoring Experiment (GOME) ozone profiles from nine different algorithms

Y. J. Meijer,[1,2] D. P. J. Swart,[1] F. Baier,[3] P. K. Bhartia,[4] G. E. Bodeker,[5] S. Casadio,[6]
K. Chance,[7] F. Del Frate,[8] T. Erbertseder,[3] M. D. Felder,[4,9] L. E. Flynn,[10]
S. Godin-Beekmann,[11] G. Hansen,[12] O. P. Hasekamp,[13] A. Kaifel,[14] H. M. Kelder,[2,15]
B. J. Kerridge,[16] J.-C. Lambert,[17] J. Landgraf,[13] B. Latter,[16] X. Liu,[7] I. S. McDermid,[18]
Y. Pachepsky,[19] V. Rozanov,[20] R. Siddans,[16] S. Tellmann,[20] R. J. van der A,[15]
R. F. van Oss,[15] M. Weber,[20] and C. Zehner[21]

[1]   An evaluation is made of ozone profiles retrieved from measurements of the nadir-viewing Global Ozone Monitoring Experiment (GOME) instrument. Currently, four different approaches are used to retrieve ozone profile information from GOME measurements, which differ in the use of external information and a priori constraints. In total nine different algorithms will be evaluated exploiting the optimal estimation (Royal Netherlands Meteorological Institute, Rutherford Appleton Laboratory, University of Bremen, National Oceanic and Atmospheric Administration, Smithsonian Astrophysical Observatory), Phillips-Tikhonov regularization (Space Research Organization Netherlands), neural network (Center for Solar Energy and Hydrogen Research, Tor Vergata University), and data assimilation (German Aerospace Center) approaches. Analysis tools are used to interpret data sets that provide averaging kernels. In the interpretation of these data, the focus is on the vertical resolution, the indicative altitude of the retrieved value, and the fraction of a priori information. The evaluation is completed with a comparison of the results to lidar data from the Network for Detection of Stratospheric Change stations in Andoya (Norway), Observatoire Haute Provence (France), Mauna Loa (Hawaii), Lauder (New Zealand), and Dumont d'Urville (Antarctic) for the years 1997–1999. In total, the comparison involves nearly 1000 ozone profiles and allows the analysis of GOME data measured in different global regions and hence observational circumstances. The main conclusion of this paper is that unambiguous information on the ozone profile can at best be retrieved in the altitude range 15–48 km with a vertical resolution of 10 to 15 km, precision of 5–10%, and a bias up to 5% or 20% depending on the success of recalibration of the input spectra. The sensitivity of retrievals to ozone at lower altitudes varies from scheme to scheme and includes significant influence from a priori assumptions.

[1]Laboratory for Environmental Measurements, Environmental Risks and Safety Division, National Institute of Public Health and the Environment, Bilthoven, Netherlands.

[2]Also at Faculty of Applied Physics, Eindhoven University of Technology, Eindhoven, Netherlands.

[3]German Aerospace Center, Wessling, Germany.

[4]NASA Goddard Space Flight Center, Greenbelt, Maryland, USA.

[5]National Institute of Water and Atmospheric Research, Lauder, New Zealand.

[6]SERCO spa, Frascati, Italy.

[7]Harvard-Smithsonian Center for Astrophysics, Cambridge, Massachusetts, USA.

[8]Dipartimento di Informatica Sistemi e Produzione, Tor Vergata University, Rome, Italy.

[9]Now at Leibniz Computing Centre, Garching, Germany.

[10]NOAA National Environmental Satellite, Data, and Information Service, Camp Springs, Maryland, USA.

[11]Service d'Aeronomie du Centre National de la Recherche Scientifique, Universite Pierre et Marie Curie Paris, Paris, France.

[12]Polar Environmental Centre, Norwegian Institute for Air Research, Tromsø, Norway.

[13]Space Research Organization Netherlands, Utrecht, Netherlands.

[14]Center for Solar Energy and Hydrogen Research, Stuttgart, Germany.

[15]Royal Netherlands Meteorological Institute, De Bilt, Netherlands.

[16]Rutherford Appleton Laboratory, Didcot, UK.

[17]Space Aeronomy Institute of Belgium, Brussels, Belgium.

[18]Jet Propulsion Laboratory, Wrightwood, California, USA.

[19]STG, Inc., Reston, Virginia, USA.

[20]Institute of Environmental Physics, University of Bremen, Bremen, Germany.

[21]European Space Agency, Frascati, Italy.

1. Introduction

[2] In this paper we will evaluate different approaches to retrieve height-resolved ozone information from spectral data of the Global Ozone Monitoring Experiment (GOME), which was launched in April 1995 on board the second European Earth Remote Sensing (ERS-2) satellite. An evaluation of the currently available retrieval algorithms becomes increasingly important with the growing volume of satellite data from past, recent and future missions. In particular, this involves the ozone profile data from nadir-viewing instruments like Solar Backscatter Ultraviolet (SBUV), SBUV/2, GOME, Scanning Imaging Absorption Spectrometer for Atmospheric Cartography (SCIAMACHY), GOME-2 and Ozone Monitoring Instrument (OMI). Some of the algorithms provide data products which include averaging kernels and a priori profile information, which can be used to characterize the retrieval. The methods used here are taken from *Meijer et al.* [2003] and *Connor et al.* [1995]. In the paper by *Meijer et al.* [2003], different methods were investigated and applied to GOME data measured around the lidar station in Lauder, New Zealand, and retrieved by the algorithm of the Royal Netherlands Meteorological Institute (KNMI). This paper will include data from nine different GOME ozone profile retrieval algorithms, and they will be compared to lidar data from five stations selected to represent different global regions.

[3] In April 2001 the European Space Agency (ESA) initiated the GOME-1 Ozone Profile Retrieval Working Group (GOME1-O3P-WG, see also http://earth.esa.int/gome1/). In five meetings spread over 2.5 years this group served as a forum for scientists working on the retrieval and validation of GOME ozone profiles. The main objectives were to develop and improve retrieval algorithms and intercomparison methods, which should ultimately enable long-term ozone trend monitoring and prepare for future mission data processing. Although in some papers two satellite retrieval algorithms have been compared [e.g., see *Müller et al.*, 2003], this paper is unique in comparing nine different retrieval algorithms applied to the same satellite irradiance measurements (level 1 data) to retrieve vertical profiles of ozone (level 2 data). All groups were provided with the same set of GOME spectral data which have been processed to ozone profiles in a uniform format and on a common altitude grid, which was requested to all participants in order to foster intercomparisons and interpretation studies. The processed data have been evaluated by independent groups (i.e., Space Aeronomy Institute of Belgium (BIRA-IASB) and Dutch National Institute for Public Health and the Environment (RIVM)) for their retrieval capabilities, data quality and particular merits. It should be clear that the scope of this evaluation paper is on characterization of these nine algorithms rather than on ranking.

[4] In section 2 we present the nine different retrieval algorithms currently available and involved in the GOME1-O3P-WG. In section 3 we present the interpretation results derived from the provided averaging kernel and a priori information. In section 4 we present intercomparison results of the GOME data with data from stratospheric ozone lidars at several strategic locations (northern/southern midlatitude, tropics, and polar region). In section 5 we present the

discussion which is followed in section 6 with final conclusions and an outlook to future work.

2. GOME Ozone Profile Retrieval Algorithms

[5] The GOME instrument [*Burrows et al.*, 1999a] measures, in nadir-viewing geometry, scattered sunlight from the atmosphere in the ultraviolet (UV), visible and near-infrared spectral regions (237–794 nm at 0.2–0.4 nm resolution). The GOME spectral range is covered by four diode array detectors. The ozone profile retrieval methods use spectral windows within bands 1a, 1b and 2 (see Figure 1), covering the range 237–406 nm. GOME scans the Earth atmosphere using a scan mirror, which rotates perpendicular to the flight direction in an angle ranging from 31° to −31° with respect to the zenith direction. This mirror takes 4.5 s to scan in one direction (forward scan) and 1.5 s to return in the opposite direction (backward scan), and during this scanning the GOME detectors are read out every 1.5 s. Nominally, this results in a swath of about 960 km covered by the scan mirror. The size of the ground pixel in the flight direction is governed by the slit opening and amounts to about 40 km. For the smallest wavelengths the obtained signal-to-noise ratio is too small during the 1.5 s integration time. Therefore part of band 1, named band 1a, is read out every 12 s corresponding to a ground pixel of 960 by 80 km². The upper wavelength limit of band 1a was at the start of mission set to 307.2 nm, but in June 1998 it was shifted to 282.9 nm (to obtain more ozone profile information for smaller ground pixels, especially tropospheric ozone). In addition, for correction of its polarization sensitivity, GOME measures the degree of polarization using three dedicated, broadband polarization measurement devices (PMDs) covering the spectral ranges 300–400, 400–600, and 600–800 nm, respectively. As the PMDs are read out every 93.75 ms, one PMD pixel covers 1/16th of every nominal pixel. This subpixel information can be used to estimate the cloud fraction [*Koelemeijer et al.*, 2001]. GOME spectra, i.e., geolocated, spectrally and radiometrically calibrated solar irradiances and earthshine radiances, have been supplied by ESA through the GOME Data Processor (GDP) [*Deutsches Zentrum für Luft- und Raumfahrt*, 1996] version 2.0 with key data version 8.5. The calibration includes a correction for the polarization sensitivity, which can be turned on or off in the codelivered extraction software.

[6] Height-resolved information of the ozone concentration can be derived from GOME measurements by exploiting the steep increase of the ozone absorption cross section from 350 to 265 nm. This information basically comes from differences in effective scattering height, as photons at the short-wavelength side are highly absorbed and carry only information on the upper altitude layers, while photons with increasing wavelength reveal information on lower layers of the atmosphere. Currently, four different approaches are followed to retrieve ozone profile information from GOME data, which differ in the use of external information, a priori constraints and exploited spectral range. Eight algorithms are based on direct inversion of the GOME measured spectra using optimal estimation (OE), Phillips-Tikhonov regularization (PTR), or neural network (NN) techniques.
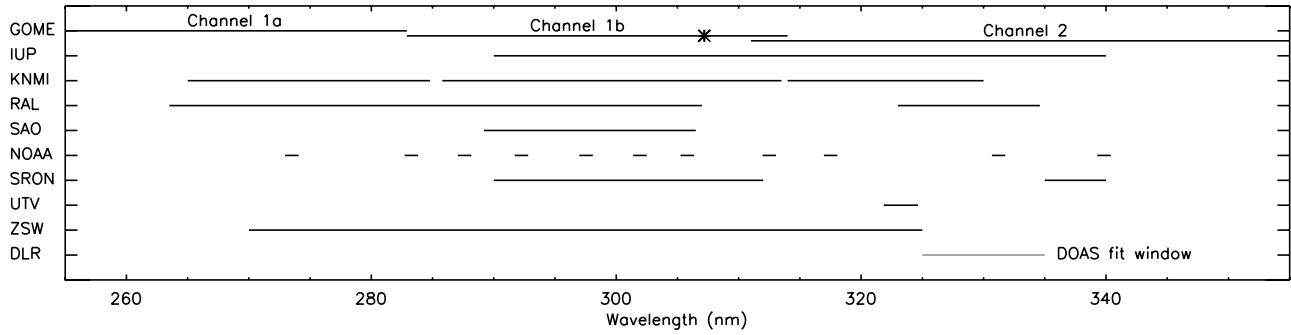
Figure 1. Wavelength ranges exploited by the nine different retrieval schemes to retrieve ozone profiles from GOME measurements (names indicated on the left). The top lines, indicated with GOME, show the ranges available from the three applicable GOME measurement bands; a change to the next band is indicated with a vertical step. The lines indicate the situation after June 1998, when the division between band 1a and 1b was changed (asterisk denotes its previous position). The DOAS fit window is indicated in gray for DLR because this algorithm only exploits the ozone column information present in the GOME spectra and not the profile information.

The ninth scheme is based on assimilation into a three-dimensional (3-D) atmospheric model of the total column ozone densities from the GOME operational level 2 product generated by Deutsches Zentrum für Luft- und Raumfahrt (DLR) on behalf of ESA, i.e., data assimilation (DA) technique. An overview of the used input parameters and main algorithm characteristics is shown in Table 1. In Table 1, coadding of pixels refers to the averaging of all band 1b and 2 spectra within the band 1a integration period, which is then combined with the band 1a spectrum to get a single measured spectrum used as input for the retrieval. This coadding ensures that for all retrieval wavelengths the detector observed the same ground scene. As the integration time of the combined spectrum is longer, the resultant measurement area (or ground pixel) is larger. The disadvantage of this approach is therefore that fewer of the larger scenes are likely to be cloud-free. Other schemes combine measurements from the 960 by 80 km^2 band 1a pixel with measurements in band 1b and band 2 at native 320 by 40 km^2 pixel size. The exploited wavelength region for each algorithm is shown in Figure 1. In Table 1 we have also indicated which algorithms used the optional GDP polarization correction or another correction scheme. In the following sections we will briefly describe the specific features and implementation method of all nine algorithms, and for further reading and more specific details the relevant references are provided.

2.1. Optimal Estimation Approach (Five Algorithms)

[7] Ozone profile retrieval from UV reflectance measurements is an ill-posed problem which can only be solved by applying suitable constraints. The well-known nonlinear OE approach outlined by *Rodgers* [2000] iteratively applies the linear OE formula to find the cost function minimum. This method can be used for the inversion of weakly nonlinear forward models, and solves ill-posed problems by using a priori information as regularization constraint. In the retrieval the spectral measurement is related to an atmospheric profile with a forward model; the use of an a priori profile and its covariance matrix stabilizes this inversion by providing suitable constraints for a solution.

[8] The retrieved ozone profile from the optimal estimation method can be regarded as a weighted average between a priori and measurement information. This is reflected in [*Rodgers*, 2000, p. 31]

$$\mathbf{x_{retrieved}} = \mathbf{A}\mathbf{x_{true}} + (\mathbf{I} - \mathbf{A})\mathbf{x_{a\ priori}}, \tag{1}$$

with the matrix $\mathbf{A}$ having elements of

$$A(z,z') = \frac{\partial x(z)_{\text{retrieved}}}{\partial x(z')_{\text{true}}}, \tag{2}$$

and for the OE methods $\mathbf{A}$ is given as [*Rodgers*, 2000, p. 67]:

$$\mathbf{A} = \mathbf{S_a}\mathbf{K^T}\left(\mathbf{K}\mathbf{S_a}\mathbf{K^T} + \mathbf{S_\varepsilon}\right)^{-1}\mathbf{K}. \tag{3}$$

[9] In these equations, $\mathbf{x_{retrieved}}$, $\mathbf{x_{a\ priori}}$, and $\mathbf{x_{true}}$ are vectors of ozone number densities at the altitude levels $z_{i=1,n}$ of the retrieval algorithm and they correspond to the values of the retrieved, a priori and true (i.e., observed) state, respectively. $\mathbf{A}$ is the so-called averaging kernel matrix, or model resolution matrix. Reorganization of equation (1) shows that $\mathbf{A}$ characterizes the mapping between (1) the difference between the true and the a priori profile (true anomaly) and (2) the difference between the retrieved and a priori profile (retrieved anomaly). In equation (3), $\mathbf{S_a}$ and $\mathbf{S_\varepsilon}$ are the a priori and measurement error covariance matrices, respectively, and $\mathbf{K}$ is the so-called weighting function matrix, which describes how the forward model ($F(\mathbf{x})$), that relates the spectral measurement to the true state vector, is sensitive to changes in the state vector, i.e., $K_{ij} = \partial F_i(\mathbf{x})/\partial x_j$.

[10] In case of ozone profile retrieval from UV spectra of nadir-viewing instruments like GOME, the averaging kernel reflects the limited sensitivity of the spectral measurement to fine-scale structures and to the profile below the ozone maximum. In addition, the kernels are dependent on the detailed specification of the state vector, a priori and measurement errors which are particular to a specific

Table 1. Overview of the Main Input Parameters and Algorithm Characteristics[a]

Algorithm Group[b]	Used Approach[b]	A Priori $O_3(z)$[c]	Correlation Length,[d] km	Temperature Profile[b]	Cloud Information[b]	O_3 Cross Sections[e]	Pixel Coadding	Polarization Corrected Spectra[f]	Radiative Transfer Model[b]
IUP	OE	F-K	5[g]	UKMO	albedo	FM	yes	GDP-extractor	GOMETRAN
KNMI	OE	F-K	4–5[g]	ECMWF[h]	FRESCO	B-P, O	yes	GOMECAL	LIDORT
RAL	OE	F-K	6–8[i]	UKMO	albedo	B-P	no	GDP extractor	GOMETRAN
SAO	OE	T-v8	6[i]	ECMWF	GOMECAT	MA	yes	GOMECAL	LIDORT
NOAA	OE	F-K[j]	~10[g]	ECMWF[h,j]	T-v8[e]	B-P	no	GDP extractor	TOMRAD
SRON	PTR	N/A	N/A	UKMO	FRESCO	V	yes	no	SRON
UTV	NN	trained	N/A	no	no	N/A	no	no	N/A
ZSW	NN	trained	N/A	UKMO	O₂ A band	N/A	no	GDP extractor	N/A
DLR	DA	column	N/A	UKMO	N/A	N/A	N/A	N/A	N/A

[a]As described in section 2. N/A, not applicable for this approach.

[b]See the appropriate subsections in section 2 for the used abbreviations (e.g., IUP, OE, UKMO, GOMETRAN, etc.).

[c]F-K, ozone climatology of *Fortuin and Kelder* [1998]; T-v8, TOMS version 8 climatology [*Bhartia and Wellemeyer*, 2002].

[d]Correlation length is used to construct the a priori covariance matrix, see equation (4) in section 2.1.

[e]O, ozone cross sections update of *Orphal* [2003]; MA, ozone cross sections of *Malicet et al.* [1995]; V, ozone cross sections of *Voigt et al.* [1999]. FM, ozone cross sections measured in laboratory on GOME flight model [*Burrows et al.*, 1999b]; B-P, ozone cross sections of *Bass and Paur* [1984] and *Paur and Bass* [1984].

[f]GDP extractor, GOME Data Processor [*Deutsches Zentrum für Luft- und Raumfahrt*, 1996] extractor option; GOMECAL, spectral recalibration tool for GDP spectra [*van Geffen*, 2004].

[g]In equation (4), $b = \frac{1}{2}$.

[h]Climatological values are used instead of analyses.

[i]In equation (4), $b = 1$.

[j]Normally, SBUV version 8 climatology [*McPeters et al.*, 2003] are used.

retrieval scheme. For example, as evident from equations (1) and (3), for smaller measurement errors the averaging kernel matrix tends toward the identity matrix and hence the OE solution becomes less dependent on the a priori profile. For larger measurement errors the averaging kernel elements go to zero and the solution relies more on the a priori. For the a priori errors the situation is reverse. Therefore the "choice" for the settings of the input measurement and a priori errors is important in the design of a retrieval system. Although there is a consensus for the measurement error, there is no such thing for the a priori. The complete a priori covariance matrix is generally constructed assuming an exponential decrease from the diagonal value (i.e., a priori variance) using a correlation length. The off-diagonal elements of $\mathbf{S_a}$ can then be written as

$$S_a(z, z') = \sqrt{S_a(z,z) \cdot S_a(z',z')}\, e^{-\left((z-z')^2/l^2\right)^b}, \qquad (4)$$

[11] with $b = 1$ or $\frac{1}{2}$, depending on whether *Rodgers* [1990, equation 16] or *Hoogen et al.* [1999, equation (3)] is followed, respectively, for the chosen functional decay. The more determining factor in equation (4) is the choice for l, which is the so-called correlation length. The distance at which the covariance has decreased by e^{-1}, from the variance at the nominal altitude, can be directly compared between schemes that use equation (4) with different values for b. This distance is reached when $(z-z')$ equals l and then allows direct comparison of l.

[12] Equation (1) reflects the deviation between the true and the retrieved profile, which is especially important when comparing the retrieved profile to correlative measurements. In the two extreme cases when (1) $\mathbf{A}$ is the identity matrix: the retrieved and the true profiles are equal, and (2) all elements of $\mathbf{A}$ are zero: the retrieved profile equals the a priori values. A detailed analysis of the averaging kernels is presented in section 3.

2.1.1. IUP Algorithm

[13] The Institute of Environmental Physics at the University of Bremen in Germany (IUP) has developed

the full retrieval method (FURM) algorithm, and data presented here stem from version 5.0. This algorithm is based on the OE method but with the addition that it includes the information matrix method from *Kozlov* [1983], which adapts the number of fit parameters to the measurement information content [*Hoogen et al.*, 1999].

[14] The radiative transfer model (RTM) GOMETRAN, specifically designed for GOME retrieval applications [*Rozanov et al.*, 1997, 1998], is used for calculating radiances and weighting functions. Besides ozone eigenvectors, other atmospheric parameters such as aerosol, temperature, NO_2, albedo, Rayleigh scattering and the so-called Ring effect are simultaneously fitted. These parameters show negligible correlation among each other. After each iteration step a shift and squeeze between the wavelength axes of radiance, irradiance and cross sections is performed for wavelength adjustments. The Ring effect, or the filling in of solar absorption lines, can be explained by rotational Raman scattering and is taken into account by using look-up tables, for various atmospheric scenarios and solar zenith angles, to correct the GDP spectra.

[15] Clouds are treated as highly reflecting surfaces at 0-km altitude (clouds as albedo approach), which means that in the RTM the spherical albedo represents the weighted mean of surface and cloud albedo, the weight being the fractional cloud cover. Initially, albedo (and hence cloud) information is derived from the PMDs, and then it is further adjusted as part of the fitting process. In the RTM the Earth's surface is assumed to be a Lambertian reflector with wavelength-dependent albedo.

[16] The GDP spectra contain unresolved problems with the radiometric calibration, particularly between 260 and 290 nm [*Hilsenrath et al.*, 1996]. In the retrieval they appear as spectral fit residuals with characteristic structures, but none of the atmospheric fit parameters can account for them [*Hoogen et al.*, 1999]. An empirical calibration correction function was derived separately for bands 1 and 2. In the retrieval algorithm third-order Chebyshev polynomials are

taken into account as additional fitting parameters using the coefficients of the correction function. Below 290 nm, there are also strong NO$_\gamma$ spectral features in the measurements [*McPeters*, 1989], which cannot appropriately be taken into account in the RTM. These two reasons lead to the restriction in the IUP algorithm (version 5.0) of only fitting wavelengths longer than 290 nm. In a more recent development, a new calibration correction scheme has been introduced that permits adding the wavelength range 275–290 nm to the fit window [*Tellmann et al.*, 2004], but this new version (6.0) was not available for this comparison.

[17] The a priori ozone profiles used in the IUP algorithm are from the global ozone climatology of *Fortuin and Kelder* [1998], which is based on ozonesonde and satellite measurements. This climatology provides monthly zonal mean ozone profiles in 10° latitude bands. The a priori variance of these profiles is fixed to 30%. The a priori covariance matrix is generated following equation (4) with $b = \frac{1}{2}$ and using a correlation length of 5 km. The temperature profiles are taken from the UK Met Office (UKMO) analysis [*Swinbank and O'Neill*, 1994], and are used to take into account the temperature dependence of the ozone cross sections.

2.1.2. KNMI Algorithm

[18] The Royal Netherlands Meteorological Institute (KNMI) developed the ozone profile retrieval algorithm (OPERA), and version 1.3 was used to generate data for this paper. Note that this algorithm is different from the retrieval algorithm described in the paper of *van der A et al.* [2002], and the main difference is the RTM used. Ozone profiles are derived from the GOME data in the wavelength range 270–330 nm, and the spectra are coadded for the data coming from band 1b and 2. The radiometric and wavelength calibration of the GDP level 1 data are too inaccurate for ozone profile retrieval, and therefore several corrections are applied using the spectral calibration program GOMECAL (available through http://www.knmi.nl/gome_fd/gomecal/). This involves an improved wavelength calibration [*van Geffen and van Oss*, 2003], an improved correction for the polarization sensitivity of GOME [*Schutgens and Stammes*, 2003] and a radiometric recalibration involving a time-independent and a time-dependent (degradation) correction [*van der A et al.*, 2002].

[19] The Sun-normalized radiances are simulated by constructing an atmospheric model and running the Linearized Discrete Ordinate Radiative Transfer model LIDORTA in six streams [*van Oss and Spurr*, 2002]; the number of streams sets the angular resolution of the model. LIDORTA is a simplified and sped-up version of the full LIDORT model [*Spurr et al.*, 2001] replacing several numerical solvers with analytical solutions. LIDORTA is only applied for the multiple scattered part of the radiance and runs with a limited set of 20 layers. The single scattering part is computed with a dedicated, simpler and therefore faster, single scattering model with the full retrieval grid of 40 layers. In the model, the ozone profile elements that are actually fitted for are layer column amounts at a fixed vertical grid. In this version of the algorithm, the layers are chosen in such a way that they have the required GOME1-O3P-WG altitude levels at their centers.

[20] LIDORTA treats the sphericity of the atmosphere both for the solar direct beam and the line of sight by a pseudospherical approximation. LIDORTA is a scalar model in the sense that it does not treat polarization and the vector nature of the radiation field. This gives errors for the radiance at the top of the atmosphere in the wavelength range used that can reach 10% for scattering angles of 90°. This error is corrected for using a precomputed look-up table containing the scalar error for the complete range of wavelengths, atmospheric and viewing conditions. Raman scattering (responsible for the Ring effect) is not treated in the RTM, but accounted for using a high-resolution spectrum convolved with the Raman lines [*Chance and Spurr*, 1997], and the amplitude for this Ring spectrum is fitted as an auxiliary parameter.

[21] The atmospheric model used in the KNMI algorithm treats (fractional) cloud cover as a Lambertian reflecting layer at the cloud top height for the fraction of the pixel covered with clouds. The effective cloud fraction and cloud top height are obtained from the Fast Retrieval Scheme for Cloud Observables (FRESCO) extracting information from the oxygen A band [*Koelemeijer et al.*, 2001]. By fitting an effective cloud fraction, the presence of aerosols is partly taken into account in the FRESCO retrieval. The error made with this procedure is smaller than when taking a (random) guess at the unknown aerosol distribution (confirmed by *Boersma et al.* [2004] for GOME NO$_2$ retrievals). The surface albedo is fitted for cloud fractions <0.15, and for all other cases the albedo of the cloud.

[22] For the ozone cross sections, OPERA uses the temperature-parameterized data set of *Bass and Paur* [1984] and *Paur and Bass* [1984], corrected according to *Orphal* [2003]. Trace gases other than ozone are not treated and assumed not to affect the retrieval in this spectral range. The a priori ozone profile information comes from the global ozone climatology of *Fortuin and Kelder* [1998], with covariance information derived from the same data set [*Bhartia*, 2002], which corresponds to a correlation length of 4–5 km in equation (4) with $b = \frac{1}{2}$.

2.1.3. RAL Algorithm

[23] The Rutherford Appleton Laboratory (RAL) has developed a three-step scheme to retrieve ozone profiles spanning troposphere and stratosphere [*Siddans*, 2002; *Munro et al.*, 1998]. Version 2.0 of the retrieval scheme was used for this paper. In step 1, an ozone profile is retrieved from Sun-normalized radiances at selected wavelengths of the ozone Hartley band (GOME band 1) in the range 265–307 nm. Information from this spectral range is primarily on stratospheric ozone. A priori ozone profile comes from the *Fortuin and Kelder* [1998] climatology except that in the troposphere a fixed value of 10^{18} molecules/m^3 is assumed (1.5–2 times larger than the climatological values). The a priori uncertainty is set by default to 100% for retrieval levels at 0, 6 and 12 km, 30% at 16km, 10% from 20–52 km, 50% at 56km, and 100% from 60–80km (retrieval levels are spaced with 4-km intervals throughout the stratosphere and mesosphere). The default uncertainty is replaced by the *Fortuin and Kelder* [1998] climatological relative variability at altitudes where the latter exceeds the former. A vertical correlation length of 6 km is applied to generate the covariance matrix using equation (4)

with $b = 1$. The surface albedo, a scaling factor for the Ring effect and the dark signal are retrieved jointly.

[24] In step 2, the surface albedo for each of the eight band 2 ground pixels is retrieved from the Sun-normalized radiance spectrum between 335 and 340 nm. Then, in step 3, information on lower stratospheric and tropospheric ozone is added by exploiting the temperature dependence of the spectral structure in the ozone Huggins bands. The wavelength range 323–334 nm (GOME band 2) is used in conjunction with UKMO analyzed temperature profiles [*Swinbank and O'Neill*, 1994]. Each direct Sun band 2 spectrum is fitted to a high-resolution (0.01 nm) solar reference spectrum to improve knowledge of wavelength registration and slit function width.

[25] In the Huggins bands fit, the log of Sun-normalized radiance is taken and a low (third) order polynomial is subtracted, allowing differential structures to be fitted to a precision of <0.1% root-mean-square (compare ~1% in the Hartley band). This differential approach in step 3 leads to improvements in the tropospheric retrieval and results in less stringent requirements on the absolute radiometric accuracy. In this step the a priori ozone profile and its error are the output from step 1, except that an a priori correlation length of 8 km is imposed.

[26] The RTM is derived from GOMETRAN [*Rozanov et al.*, 1997], but the original code has been modified substantially in order to increase its efficiency without losing accuracy. Within the RTM there is no explicit representation of clouds, which are treated as highly reflecting surfaces at 0-km altitude (clouds as albedo approach, see section 2.1.1). When clouds are present, a negative bias in retrieved ozone below the actual cloud top height is therefore to be expected from this scheme.

2.1.4. SAO Algorithm

[27] The Smithsonian Astrophysical Observatory (SAO), a research institute of the Smithsonian Institution, is a part of the Harvard-Smithsonian Center for Astrophysics (CfA). The SAO algorithm, version 0.9, also uses the OE approach to derive ozone profile information. This algorithm performs a detailed treatment of (1) variable slit width in the instrument transfer function, (2) variable wavelength shift between radiances, irradiances and spectroscopic data, (3) real-time first-order Ring effect correction [*Sioris and Evans*, 2000], (4) undersampling correction [*Chance et al.*, 2005], and (5) polarization correction.

[28] Ozone profiles are retrieved from GDP data with the GOMECAL polarization correction only (i.e., not using the other GOMECAL correction options). To reduce measurement errors and because of relatively broad ozone absorption structure in 289–307 nm, five neighboring pixels (i.e., in wavelength grid) are coadded and sampled at every 2 pixels. LIDORT [*Spurr et al.*, 2001] is used to simulate radiances and weighting functions with similar polarization correction to the KNMI algorithm. The state vector includes ozone number density at 26 levels of 2 km from 0– to 50–km altitude, surface albedo, scaling parameters for Ring effect and undersampling correction, and scaling and shift parameters for other trace gases (NO$_2$, SO$_2$, BrO).

[29] In the characterization of the atmosphere, the SAO algorithm uses monthly mean stratospheric aerosol data from SAGE-II [*Bauman et al.*, 2003] and tropospheric aerosol model fields from the Global Ozone Chemistry Aerosol Radiation and Transport (GOCART) model [*Chin et al.*, 2002] as described by *Martin et al.* [2003]. Clouds are treated as Lambertian surfaces, and cloud fraction and cloud top pressure come from the GOME cloud retrieval algorithm (GOMECAT, which was formerly abbreviated as CRAG) [*Kurosu et al.*, 1999]. An initial surface albedo is derived from the spectral measurements at 370 nm, where atmospheric absorption is minimal. The SAO algorithm uses daily European Centre for Medium-Range Weather Forecast (ECMWF) temperature profiles and National Centers for Environmental Prediction/National Center for Atmospheric Research (NCEP/NCAR) surface pressure. The Total Ozone Mapping Spectrometer (TOMS) version 8 ozone profile climatology [*Bhartia and Wellemeyer*, 2002] with Earth-Probe TOMS monthly mean total ozone is used to initialize a priori ozone profiles. This climatology has 3–10 profiles for each 10° latitude band and month, and the Earth-Probe TOMS monthly mean total ozone is used to select the appropriate a priori ozone profile from this data set. The a priori standard deviations are based on a 15 year ozone profile climatology, from SAGE and ozonesonde data [*McPeters et al.*, 2003], with the following changes: the standard deviations at 40–50 km are assumed to be 70, 60, 50, 40, 30, 20% for 50, 48, 46, 44, 42, 40 km, respectively; and between 0 and 10 km, the a priori standard deviations are required to be at least 40%. The off-diagonal elements of the covariance matrix are generated using equation (4) with $b = 1$ and a correlation length of 6 km. In addition, the ozone profiles above 50 km are fixed using climatological values [*Bhartia and Wellemeyer*, 2002].

2.1.5. NOAA Algorithm

[30] The National Oceanic and Atmospheric Administration (NOAA) has applied the version 8 SBUV/2 algorithm, developed for the SBUV instruments, to the GOME data. Version 8 was derived from the version 6 algorithm which is described by *Bhartia et al.* [1996]. Unlike the previous four OE algorithms, this algorithm was not specifically designed for GOME data. The SBUV data are measured at the following wavelengths (nm): 251.99, 273.51, 283.27, 287.62, 292.26, 297.54, 301.93, 305.80, 312.50, 317.51, 331.23, and 339.84 with a bandwidth of ~1.1 nm. A triangular filter centered at those values has been used to convert GOME spectral data to the SBUV band pass. Because the GOME data have large errors below 270 nm, an extrapolation was used to provide the standard input for the SBUV retrieval algorithm at 251.99 nm.

[31] The SBUV algorithm uses a single-scattering forward model calculation coupled with adjustments from multiple scattering tables created from the RTM developed for TOMS, called TOMRAD. This model is based on successive iteration of the auxiliary equation in the theory of radiative transfer developed by *Dave* [1964]. This solution accounts for all orders of scattering, as well as the effects of polarization, by considering the full Stokes vector in obtaining the solution. However, the solution is limited to Rayleigh scattering only and can only handle reflection by Lambertian surfaces. Modifications that have been incorporated into the code include a pseudospherical correction, molecular anisotropy [*Ahmad and Bhartia*, 1995], and rotational Raman scattering [*Joiner et al.*, 1995]. In the

pseudospherical correction, the incoming and the outgoing radiation is corrected for changing solar and satellite zenith angle due to Earth's sphericity but the multiple scattering takes place in plane parallel atmosphere. Comparison with a full-spherical code indicates that this correction is accurate to 88° solar zenith angle [*Caudill et al.*, 1997]. For the cloud calculations, the algorithm uses an 1° × 1° climatology of monthly cloud top pressures [*McPeters et al.*, 2003], and a similar snow/ice climatology. If snow or ice is present the clouds are treated as though they are at the surface.

[32] The version 8 SBUV(/2) algorithm has its own a priori ozone [*McPeters et al.*, 2003] and temperature profile database, but they were not used for the retrieved data in this paper. For this study, the NOAA algorithm used the a priori profiles supplied by KNMI (i.e., from *Fortuin and Kelder* [1998] and ECMWF analysis for ozone and temperature, respectively). The a priori covariance is constructed as follows: the diagonal elements correspond to 50% variance and the nondiagonal covariance elements fall off with a correlation length of approximately two Umkehr layers (~10 km), using equation (4) with $b = \frac{1}{2}$. The measurement covariance is diagonal and corresponds to radiance errors of 1% in each band.

2.2. Phillips-Tikhonov Regularization Approach (One Algorithm)

2.2.1. General Description

[33] The PTR approach [*Phillips*, 1962; *Tikhonov*, 1963] has been little used for the analysis of atmospheric spectra, e.g., to retrieve ozone profiles. However, it has been extensively studied in the mathematical field of inversion. The analysis of the fundamental problem by *Hansen and O'Leary* [1993] and *Hansen* [1994] provides a basis for the application of PTR to remote sensing problems. In contrast to the OE approach, the PTR approach does not require a priori ozone profiles and corresponding covariance matrices, but uses a smoothness constraint to determine the amount of information that can be retrieved from the measurement. Nevertheless, the same equations (1) and (2) are applicable, but here the vector $\mathbf{x}_{a\ priori}$ is zero.

2.2.2. SRON Algorithm

[34] The inversion model of the algorithm developed by the Space Research Organization Netherlands (SRON) treats the ill-posed problem of ozone profile retrieval using the PTR approach [*Hasekamp and Landgraf*, 2001]. In addition to the least squares minimization between forward model and measurement, this algorithm includes minimization of the first derivative norm of the profile as a side constraint. The minimization of the least squares condition and the minimization of the first derivative norm are balanced by a regularization parameter. The rationale behind the minimization of the first derivative norm as a side constraint is that the measurement is insensitive to fine-scale structures of the ozone profile. These vertical structures do not influence the residual norm but strongly influence the first derivative norm. The regularization parameter should be chosen such that the retrieved profile contains vertical structures that most significantly influence the measurement, while the structures to which the measurement is insensitive should be filtered out. Such a value of the regularization parameter is found from the L curve [*Hansen and O'Leary*, 1993], which is a parametric

plot of the first derivative norm versus the least squares norm that has an L-shaped corner. The regularization parameter corresponding to the corner of the L curve yields a good balance between the two minimizations.

[35] The forward model of the SRON algorithm consists of a RTM based on the Gauss-Seidel iteration technique, which fully includes multiple scattering and polarization. This model simultaneously calculates the four Stokes parameters at the top of the atmosphere and the corresponding analytical weighting functions, which are essential for any physically based retrieval algorithm. The RTM is described in detail by *Landgraf et al.* [2001] for the scalar case and the extension to polarization is described by *Hasekamp and Landgraf* [2002a]. The inclusion of polarization in the radiative transfer calculations overcomes errors of up to 10% made by the commonly used scalar RTMs, which generally neglect the polarization properties of light. Another advantage of this RTM is that it allows a direct modeling of the polarization-sensitive GOME measurement using the Mueller matrix formalism. Therefore the SRON algorithm can be directly applied to the GOME measurements, which are thus not corrected for polarization (see Table 1). In this way the SRON algorithm is independent of the (optional) polarization correction of the GOME data processor, which can cause errors in the GOME spectra of up to 8% [*Hasekamp et al.*, 2002].

[36] The additional fit parameters included in the SRON algorithm are a Lambertian surface albedo, a wavelength shift to correct for calibration errors, and the amplitude of a Ring spectrum precalculated by the code of *Landgraf et al.* [2004]. The effect of clouds is accounted for by using the independent pixel approximation, which separates the radiative transfer calculations for the cloudy and the cloudless scenes, with cloud fractions and cloud top heights from FRESCO. The ozone cross sections used in the SRON algorithm are those described by *Voigt et al.* [1999].

2.3. Neural Network Approach (Two Algorithms)

[37] The NN approach uses a fully feed forward neural network, also called multilayer perceptron (MLP) [*Rumelhart et al.*, 1986], which can be applied to generate a mapping between GOME spectral data, other supplementary input parameters and the output ozone distribution. A training data set is used to derive the mapping between various input parameters and the known collocated ozone distributions. Unlike the other retrieval schemes, which use a physical approach, this approach uses all available information in a primarily statistical way. One of the main advantages of the NN is that once it is trained, which is a slow process, it is several orders of magnitude faster than the other approaches. The main disadvantage, or restriction, is the reliance on the training data set, which should be large in volume and of the highest available quality, in terms of accuracy, precision and vertical resolution. The data quality of the NN output can never be better than the quality of the training data.

2.3.1. UTV Algorithm

[38] Tor Vergata University (UTV) has developed a NN scheme to derive ozone profiles from GOME spectra. The underlying idea of the algorithm is to train a NN using already existing RAL retrieved ozone profiles [*Munro et al.*, 1998] and to use the trained net for new estimations [*Del*

Frate et al., 2002]. The method takes advantage of both the high retrieval accuracy characterizing the profiles provided by RAL, and of the potentialities of the NN which after the training process is able to give new estimations in real time. Although there are better training data sets available and the data quality of the UTV algorithm will never be better than the RAL data, the advantage of using these data is its large volume for training and perfect match in collocation. It should be noted that the RAL products used in the construction of the UTV algorithm are different (older version) from those presented by RAL in this paper.

[39] The GOME data used in the scheme consist of solar irradiance and Earth radiance spectra from GDP. The solar irradiance spectra are measured daily by GOME and are used as the reference light source spectra. The selected wavelength range is 321–325 nm with a spectral resolution of 0.12 nm, which is based on a spectral calibration performed using a fourth-order polynomial and has been chosen according to four requirements. First, in this range, there is a higher spatial resolution, with respect to the Hartley ozone absorption band, due to a shorter integration time. Second, this range is characterized by a high value of the signal-to-noise ratio. Third, in this range, there is a high-temperature dependence of the ozone cross sections [*Burrows et al.*, 1999b]. Fourth, in this range, there is the possibility to compute the ozone slant path content using the Temperature Independent Differential Absorption Spectroscopy (TIDAS) method [*Zehner and Casadio*, 2000].

[40] The Earth radiance spectra also undergo a normalization procedure in order to eliminate as much as possible the effects of instrumental parameters on the spectral shape. As far as the topology of the NN is concerned, a MLP-type network with one hidden layer is considered. The input vector consisted of the 26 selected GOME channels plus the solar zenith angle and the ozone slant path, and also the hidden layer has 28 units. Minimization of the error function has been pursued by a scaled conjugate gradient (SCG) algorithm [*Müller*, 1993].

2.3.2. ZSW Algorithm

[41] The Center for Solar Energy and Hydrogen Research (ZSW) in Stuttgart, Germany, has developed a NN scheme called Neural Network Ozone Retrieval System (NNORSY), and version 1.2 was used to generate data for this paper. In contrast to the UTV approach, the nonlinear regression performed in the ZSW algorithm infers the vertical distribution of ozone from a combination of climatological (latitude, season), meteorological (temperature) and spectral information (GOME spectra, solar zenith angle, scan angle, sensor age) [*Müller et al.*, 2003; *Müller*, 2002]. The system effectively learns to correlate the behavior of atmosphere and sensor, even as the sensor characteristics slowly change over time due to, e.g., degradation. Thus only the basic GDP calibration procedure for level 1 data is performed. ZSW algorithm employs about 100 GOME spectral values covering the wavelength ranges 290–325 nm (Hartley/Huggins band), 380–385 nm (atmospheric window), 598–603 nm (Chappuis band), and 758–772 nm (oxygen A band) [*Müller et al.*, 2003]. Employing additional cloud or ground albedo information was found to be unnecessary.

[42] UKMO analyzed temperature profiles [*Swinbank and O'Neill*, 1994] were included as a predictor, since the stratospheric part of the atmospheric temperature field is known to correlate strongly with ozone. In a NN the effect of using temperature information is quite different from the usage in an RTM, where only its comparatively small effect on ozone absorption can be exploited.

[43] In the ZSW algorithm the MLP is trained by means of a modified Resilient Propagation algorithm [*Riedmiller*, 1994], which is a fast heuristic approximation for a second-order function minimization scheme [*Bishop*, 1995]. Knowledge about the "true" ozone profile, which is needed as the MLP training target, is not derived from another GOME retrieval algorithm, but rather from collocated, highly accurate ozone measurements taken from different moments in GOME's lifetime and geographical coverage. These measurements stem from ozonesondes provided by the World Ozone and Ultraviolet Radiation Data Center (WOUDC) [*Hare et al.*, 2004] and the Southern Hemisphere Additional Ozonesondes (SHADOZ) campaign [*Thompson et al.*, 2003], as well as from the Polar Ozone and Aerosol Measurement III (POAM-III) [*Lumpe et al.*, 2002], Stratospheric Aerosol and Gas Experiment II (SAGE-II) [*Wang et al.*, 2002] and Halogen Occultation Experiment (HALOE) [*Russell et al.*, 1993] occultation sounders.

[44] The data used for the training of this NN are similar to those that are the basis for the climatologies used as a priori information in the OE retrieval algorithms (described in section 2.1). For the ZSW algorithm, unlike the OE algorithms, there is no need to average them into, e.g., monthly means, thereby destroying information. The ill-posed problem facing classical retrieval schemes is circumvented through the use of the nonspectral input data. In particular, in areas where there is little information from the satellite spectra (compare section 3.5), the MLP automatically estimates the ozone profile on the basis of its nonspectral input parameters. In other words, it behaves like a dynamical, continuous, temperature-dependent climatology, rather than a fixed a priori data set.

2.4. Data Assimilation Approach (One Algorithm)
2.4.1. General Description

[45] GOME is primarily used to retrieve total ozone column densities from a spectral window around 330 nm using the Differential Optical Absorption Spectroscopy (DOAS) technique. In order to derive ozone profiles and a daily global three-dimensional (3-D) ozone analysis, the column observations are assimilated into a 3-D chemical transport model (CTM). While the CTM is driven by meteorological wind and temperature fields, the GOME observations are sequentially assimilated into the model using an optimal interpolation scheme [e.g., *Khattatov et al.*, 2000]. The vertically integrated total column contents of the model are considered as the first-guess values. The analyzed column values are then vertically distributed weighted by the corresponding (first-guess) model profile (i.e., in ozone mixing ratios). The assimilation scheme accounts for time of observation, for spatial weighting between observation and grid, and for model and observation errors. By applying this method a global synoptic 3-D ozone analysis is available every 6 hours. Unlike the other

approaches, this approach does not use the profile information in the GOME spectra, which makes it an interesting addition, as it represents the complete a priori knowledge of the ozone vertical distribution considering all relevant chemical and physical processes, and the meteorological analyses.

2.4.2. DLR Algorithm

[46] For the assimilation approach the German Aerospace Center (DLR) uses the 3-D global CTM called ROSE/DLR. It is based on the ROSE model described in detail by *Rose and Brasseur* [1989]. An updated model version (2.7) was applied to generate the data presented in this paper [*Thomas et al.*, 2003]. This model covers all relevant gas-phase stratospheric chemical processes including oxygen, hydrogen, carbon, nitrogen, chlorine, and bromine species. Heterogeneous processes on polar-stratospheric clouds and on sulfate aerosols are also included in the model. For the assimilation of GOME total ozone column observations, the model in the DLR algorithm is run with a 5.6° × 5° longitude-latitude spatial discretization, and consists of 37 equally spaced levels covering the altitude range 8–56 km. The basic time step of the CTM is 1 hour, and therefore all GOME observations within this interval are binned. Assimilation is performed using the wind and temperature fields derived from 24-hour analyses of the UKMO following *Swinbank and O'Neill* [1994].

[47] The optimal interpolation applied for the sequential data assimilation considers the time of observation, the spatial weighting between observation and grid, the model errors, and the observation errors. At each assimilation time step, the model's volume mixing ratios are integrated to total column values, which are then interpolated to the observation space, that is the geolocation of the GOME total column observations. In a next step the observational increments (i.e., departures from the model) are determined. The linear weight matrix operator (or gain operator) transforms the resulting innovations back to the model space [*Daily*, 1991], which takes into account the spatial weighting and error information of both the observations and the model. In the final step, the analyzed total columns are vertically redistributed weighted by the first-guess model profiles. For this study, the model's first guess and GOME observation errors are set to 18% and 4%, respectively. Error covariances are parameterized by hyperbolic functions depending on the horizontal distance between the model grid point and the observation [*Riishøjgaard*, 1998]. A correction for the model bias is applied offline, which is based on zonal mean seasonal comparison results with SAGE-II data from 1996 [*Wang et al.*, 2002]. Contrary to the other approaches evaluated in this paper, this method delivers global synoptic 3-D ozone analyses every 6 hours. For the results used in this paper, daily mean values are provided.

2.5. Summary of the Different Algorithms

[48] In this section we have presented four different approaches to the retrieval of ozone profiles from GOME spectra. Five of the algorithms exploit the OE approach, each of which makes distinct assumptions which have important implications for the final retrieved profile. There is no OE method with exactly the same a priori ozone profile and related error covariance matrix. The IUP and NOAA methods use relatively large a priori error covariances everywhere, and RAL only in the troposphere and upper stratosphere, while KNMI and SAO use smaller error values.

[49] The OE- and PTR-based algorithms, physical-based approaches, strongly depend on the accuracy of the spectral calibration, and we have seen different ways of correcting the inadequate accuracy of the spectra delivered by GDP, including both calibration and polarization corrections. Obviously, these corrections significantly impact the ozone profile retrieval, and various analyses have been performed to quantify this effect for GOME and GOME-type instruments [see, e.g., *van der A et al.*, 2002; *Bhartia*, 2002]. Furthermore, the treatment of clouds, the ozone cross sections used, the inclusion of other trace gases in the fitting process, and the exploited wavelength range are tackled in different ways. In the following sections we will investigate the implications of some of these assumptions by evaluating the retrieved data products of all these algorithms.

[50] We have described two NN-based methods; the UTV algorithm trained with (RAL retrieved) ozone profile data of the nadir-viewing instrument GOME, and the ZSW algorithm trained with sonde data and relatively high-resolution satellite data (from limb-viewing occultation instruments). The ninth algorithm is based on assimilation of GOME ozone column data into a chemical transport model driven by meteorological analyses (wind and temperature fields).

3. Interpretation of GOME Ozone Profiles

3.1. Introduction

[51] The interpretation of the retrieved data products is nontrivial and requires special attention. Six of the GOME ozone profile retrievals deliver averaging kernels in their product of which five also use an a priori profile. This extra information in the data can help to interpret the retrieved ozone profiles (for an overview, see *Rodgers* [1990, 2000]). For the interpretation presented here, we focus on the three parameters proposed by *Meijer et al.* [2003], i.e., looking at the aspects of vertical resolution, the indicative altitude of the retrieved value, and the fraction of a priori information. Although the focus is the same, here a different definition of a priori fraction is used, following *Connor et al.* [1995]. The interpretation parameters are derived for the retrieved GOME data collocated with the five stations selected for the intercomparison analysis (section 4). In this paper data were selected that were measured near the lidar stations of Andoya (Norway), Observatoire Haute Provence (OHP) (France), Mauna Loa (MLO) (Hawaii), Lauder (New Zealand), and Dumont d'Urville (Antarctic) in the years 1997–1999 (see Table 2). The location of these five stations is such that the analysis will include polar, midlatitude and tropical cases. The conclusions regarding the derived interpretation parameters will be presented in section 3.6.

[52] As the NN and DA schemes considered here do not supply averaging kernel information, the data from these approaches will not be considered in this section. Nevertheless, in the paper of *Müller et al.* [2003] an attempt was made to estimate the vertical resolution of the ZSW algorithm, and they found a resolution of 3–5 km in the altitude range 15–32 km. Above 30-km altitude, they concluded

Table 2. Details of Lidar Stations Providing Correlative Data, Including Their Principle Investigator[a]

Location	Latitude	Longitude	Principle Investigator	Pairs 1997	Pairs 1998	Pairs 1999
Andoya (C)	69.30°	16.00°	G. Hansen	30	19	–
Observatoire Haute Provence (P, R)	43.94°	5.71°	S. Godin-Beekmann	135	120	35
Mauna Loa Observatory (P, R)	19.54°	−155.58°	I. S. McDermid	17	33	12
Lauder (P, R)	−45.04°	169.68°	D. P. J. Swart	92	18	13
Dumont d'Urville (P, R)	−66.67°	140.01°	S. Godin-Beekmann	22	17	–

[a]The stations are ordered from north to south. P, NDSC primary station; C, NDSC complementary station; R, system equipped with Raman detection channels for more accurate ozone profile measurements <20-km altitude.

that the resolution was mainly limited by the training data set used.

3.2. Kernel Transformation of True Profile

[53] As an illustration of the importance of considering additional information, the same ozone profile has been transformed using equation (1) with the averaging kernel and the a priori profile coming from the six different algorithms (see Figures 2a and 2b). The profile used in Figure 2 was constituted from collocated lidar and sonde data measured at Lauder, New Zealand (see section 4.2.3 for definition and selection of collocated data). An example of just one data set is shown in Figures 2a and 2c, while Figures 2b and 2d illustrate the spread obtained from applying the kernels and a priori profiles from the results of six different retrieval schemes (on the same GOME data). Bear in mind that Figure 2 does not show retrieved profiles, but instead it shows the interpretation or "translation" of how each algorithm observes the (same) "true" profile. There are some obvious differences between the transformed profiles, some of which may be attributed to the use of different a priori information or spectral ranges. In order to fully understand the observed differences, we will now look at the three previously mentioned aspects of the averaging kernels. The matrix elements described in equation (2) reflect the response of the retrieved quantity to a unit change in the true state at different altitudes. It is important to recognize that, although dimensionless, off-diagonal elements of the kernels depend on the assumed unit of perturbation. In most of the analysis here, "fractional" kernels are used which are expressed in terms of changes at each altitude relative to a nominal profile, assumed here to be equivalent to the a priori profile.

$$A_{\text{fractional}}(z, z') = \frac{x(z')_{\text{nominal}}}{x(z)_{\text{nominal}}} A(z, z'), \tag{5}$$

Hereafter $\mathbf{A_{fractional}}$ will be written as $\mathbf{A_{fr.}}$. The implication of this (common) choice of averaging kernel representation is discussed in section 3.7.

3.3. Vertical Resolution

[54] *Meijer et al.* [2003, section 4] regarded the resolving length as the most appropriate choice to estimate the vertical resolution of an averaging kernel. This quantity properly takes into account both the negative and positive contributions in the averaging kernel, gives values for all shapes of kernels, and separates the effect that some kernels have dislocated centers. The resolving length $r(z)$ or "spread about the center" is defined as

$$r(z) 12 \frac{\int [z' - c(z)]^2 A_{fr.}^2(z, z') dz'}{\left(\int A_{fr.}(z, z') dz'\right)^2}, \tag{6}$$

where the center $c(z)$ is given by [*Rodgers*, 2000, pp. 55 and 77]

$$c(z) \frac{\int z' A_{fr.}^2(z, z') dz'}{\int A_{fr.}^2(z, z') dz'}. \tag{7}$$

In these equations, z is the nominal altitude. The quantity $c(z)$ can be regarded as the centroid of a kernel, and this is the subject of section 3.4. We have applied this definition for vertical resolution and calculated the resolving lengths for the data of the six algorithms, results are shown in Figures 3a and 3b. In Figures 3a and 3b the different algorithms are presented from left to right, and the data collocated with different stations are presented from the top to the bottom for locations ranging from the Arctic to the Antarctic, respectively. Differences in number of coincidences between algorithms at a certain station are due to different number of successful retrievals, as each algorithm started with the same set of GOME level 1 data.

3.4. Indicative Altitude of Retrieved Value

[55] In the ideal case, the sensitivity of $x_{\text{retrieved}}(z)$ would be centered on (and narrowly spread about) the corresponding nominal altitude, z, but this may however not always be the case. In particular at low altitudes the retrieval may be more sensitive to perturbations in the ozone profile above. Although the averaging kernels directly reflect the vertical sensitivity of each retrieved level, it is useful for interpretation purposes to derive a figure of merit which indicates the altitude to which a particular retrieved value is predominantly sensitive. *Meijer et al.* [2003] proposed the use of the centroid of a kernel which results from applying equation (7). We have applied this definition and calculated the centroids for the data of the six algorithms, and the results are shown in Figures 4a and 4b. If the kernels are symmetric about their peak, the centroids will generally coincide with the altitudes of the peaks. However, it should be noted that kernels are always truncated at zero altitude (there is no sensitivity to "altitudes" below the surface). For kernels which correspond to low-altitude retrieval levels, this truncation means that the centroid will always be above the nominal retrieval altitude, even in the ideal case of, e.g., a triangular kernel which peaks at the retrieval level. The extent of this effect depends upon the width of the kernel.

### 3.5. Contribution of a Priori Information

[56] All retrieval schemes use regularizing information in one form or another to arrive at a stable solution or retrieval
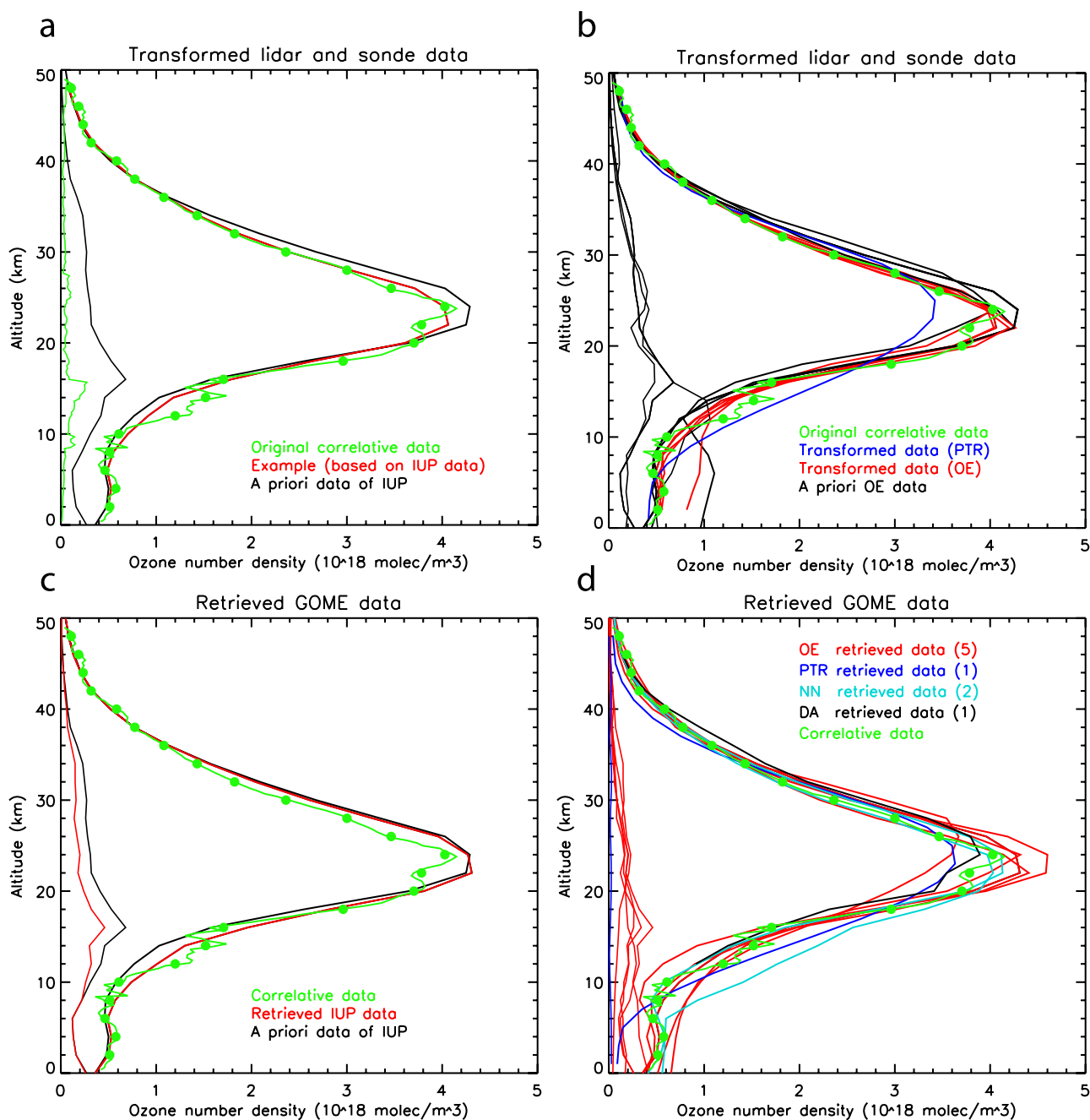
Figure 2. Figures 2a (an example) and 2b (all) show a combined sonde and lidar ozone profile (green) transformed with averaging kernels and (if applicable) a priori information of GOME data measured on the same day and processed with six different algorithms. A priori and transformed profiles are plotted with black and red lines, respectively, and the green dots represent the sonde-lidar data on the common altitude grid. Errors are plotted with corresponding colors, but with thin lines. Figures 2c (an example) and 2d (all) show for the same day again the sonde-lidar ozone profile (green), but they are now plotted with the retrieved profiles of the OE method (red), the PTR method (blue), the NN method (light blue), and the DA method (black) and their corresponding errors (thin lines and the same color) with the absence of the NN data errors. GOME and correlative data are from single retrievals measured on 24 March 1997 near Lauder, New Zealand (with a cloud fraction of 0.07); see section 4.2.3 for collocation criteria.

result. For the DA and NN approaches it is difficult to estimate in which way this additional information, instead of the actual measurement information, is in the retrieved product. For the PTR and OE approaches, the contribution

of a priori information is apparent in the retrieval product in two different ways. First, there is a smoothing term which arises from the applied regularization parameter for the PTR methods and the a priori covariance matrix (correlation
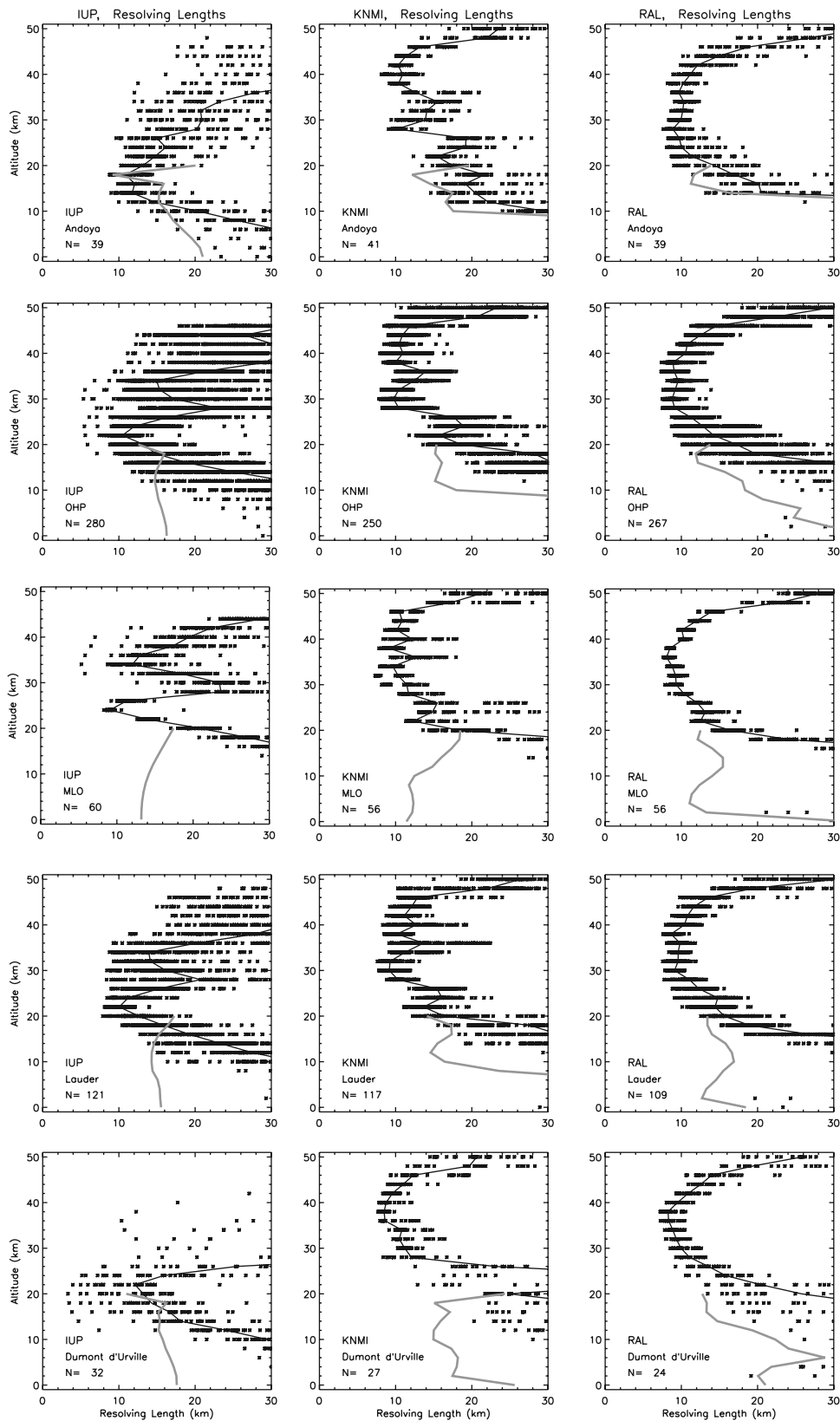
Figure 3a. Resolving lengths (asterisks) for retrieval results of three different algorithms near the lidar stations at Andoya, Observatoire Haute Provence (OHP), Mauna Loa (MLO), Lauder, and Dumont d'Urville, shown from the top downward ranging from north to south, respectively. See section 4.1 for location details and section 4.2.3 for collocation criteria. Black line shows the median values; for explanation of gray line, see section 3.7.
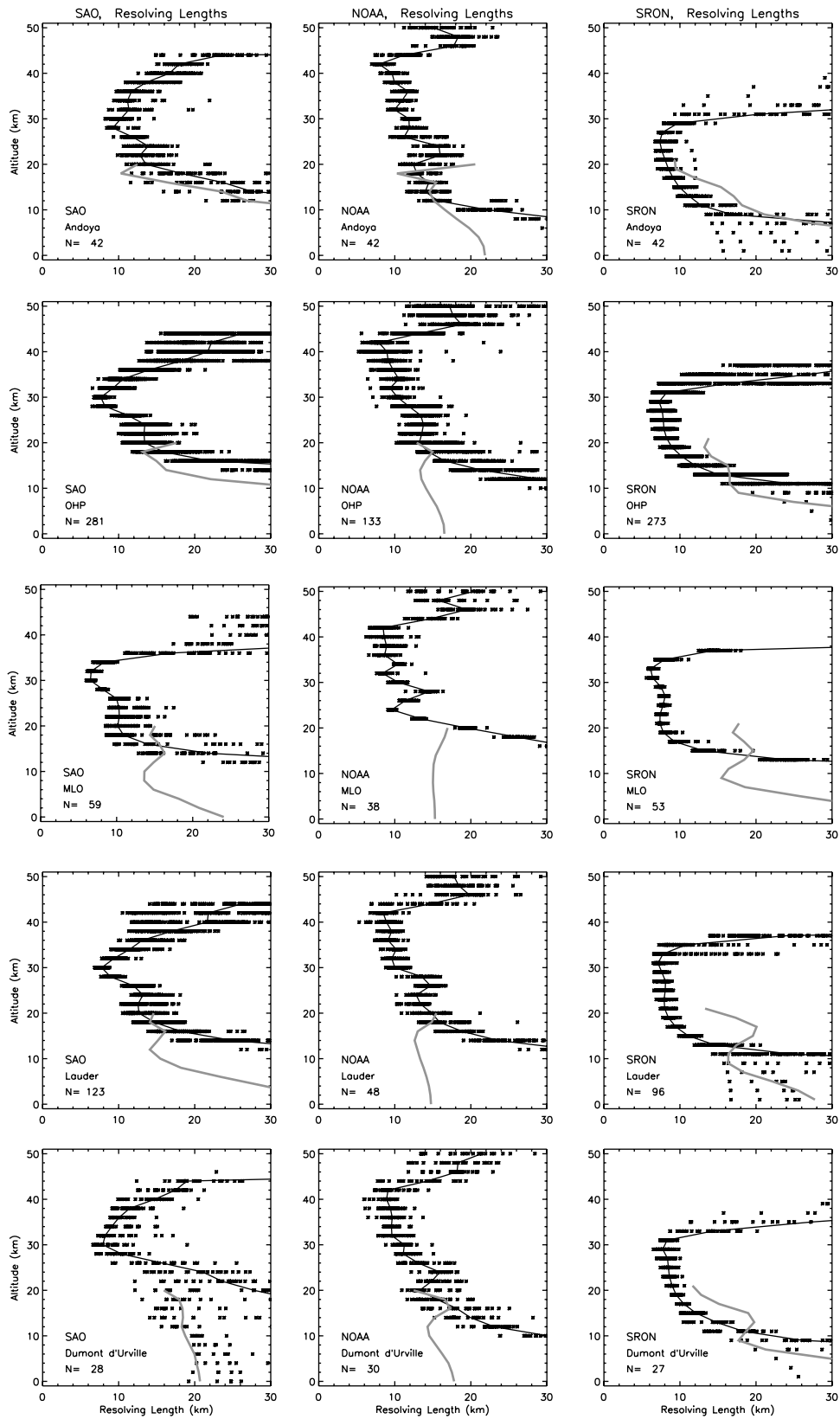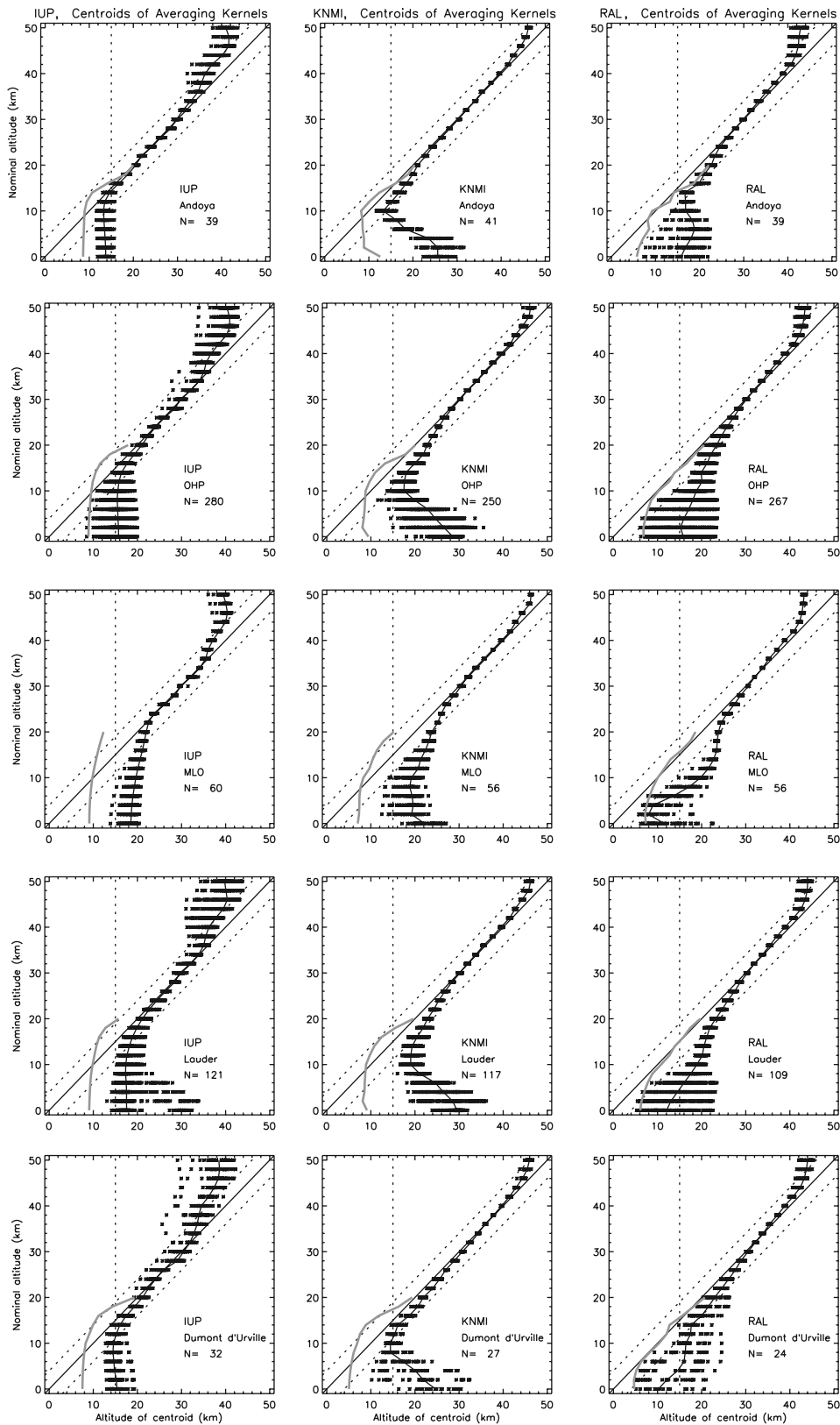
Figure 3b. Same as Figure 3a, but now showing the results for three other algorithms.

Figure 4a. Centroids of averaging kernels (asterisks) from retrieval results of three different algorithms near the lidar stations at Andoya, OHP, MLO, Lauder, and Dumont d'Urville, shown from the top downward ranging from north to south, respectively. See section 4.1 for location details and section 4.2.3 for collocation criteria. Black line shows the median values; for explanation of gray line, see section 3.7. Dotted lines serve as visual references; a vertical line at 15 km and two diagonal lines corresponding to ±4 km shift of the nominal altitude.
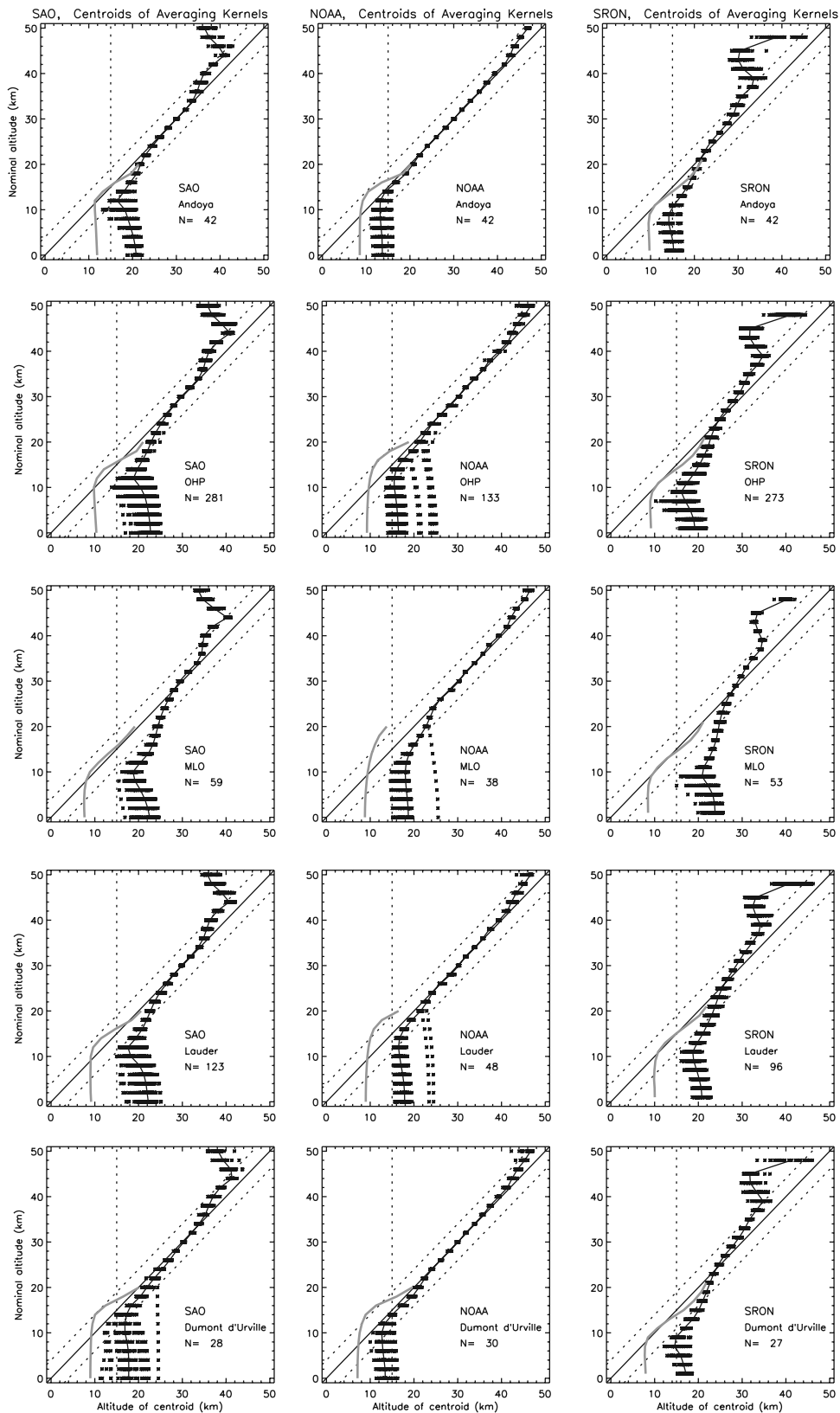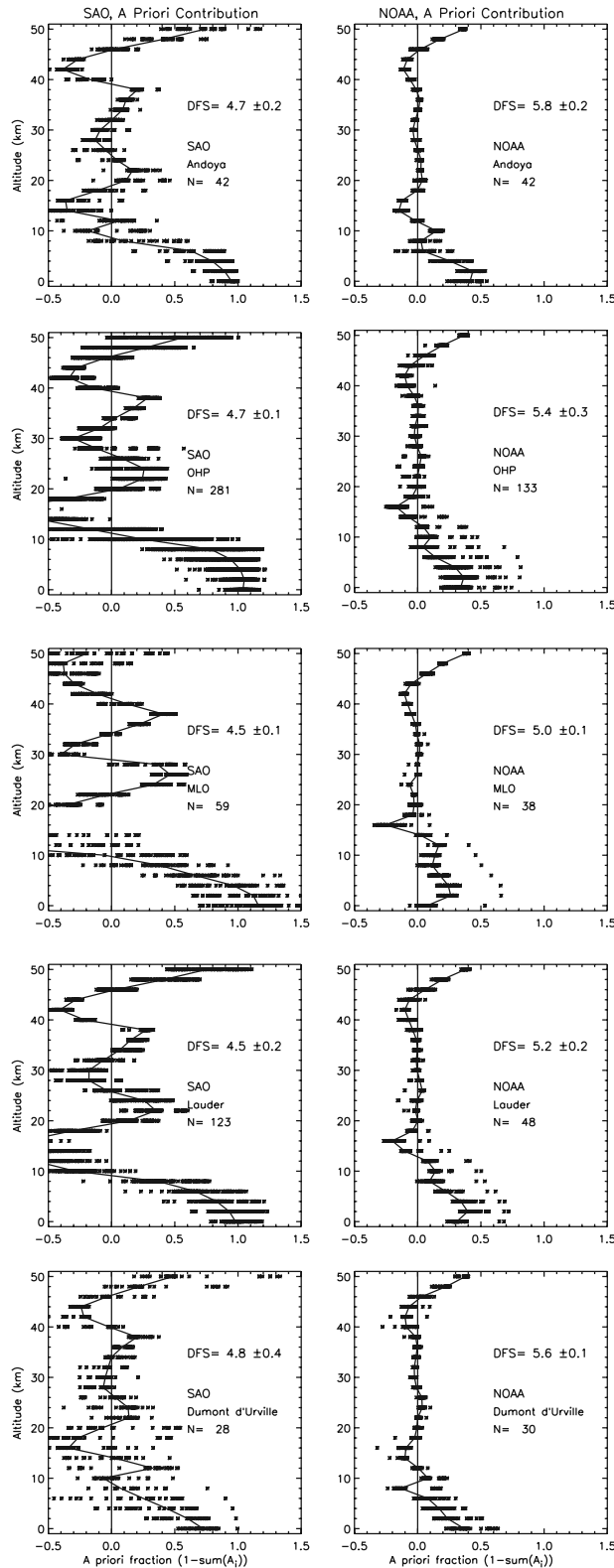
Figure 4b. Same as Figure 4a, but now showing the results for three other algorithms.

Figure 5a. A priori fraction (asterisk) in retrieval results of three different algorithms near the lidar stations at Andoya, OHP, MLO, Lauder, and Dumont d'Urville, shown from the top downward ranging from north to south, respectively. See section 4.1 for location details and section 4.2.3 for collocation criteria. Black line shows the median values.

Figure 5b. Same as Figure 5a, but now showing the results for two other algorithms.

here the focus will be on the second term, which will hereafter be called a priori fraction.

[57] Unlike the PTR approach, the retrieval algorithms based on the OE approach include a fraction of the a priori profile in the retrieved ozone values. A measure for this fraction can be estimated by calculating

$$
\text{A\_priori\_fraction}(z) = \frac{\displaystyle\sum_{i=1}^{n\_\text{levels}} \left[I(z, z_i) - A_{fr}(z, z_i) \right]}{\displaystyle\sum_{i=1}^{n\_\text{levels}} A_{fr}(z, z_i) + \sum_{i=1}^{n\_\text{levels}} \left[I(z, z_i) - A_{fr}(z, z_i) \right]}
$$

$$
= 1 - \sum_{i=1}^{n\_\text{levels}} A_{fr}(z, z_i), \tag{8}
$$

where $A_{fr}(z, z_{i=1,2,.,n\_\text{levels}})$ is the fractional kernel of level z. Equation (8) was used by *Connor et al.* [1995, section 2.5], and also *Rodgers* [2000, section 3.1.5] suggests that it can be regarded as a rough measure of the a priori fraction in the retrieval. In equation (1) the retrieved profile is expressed as a linear combination of the true and a priori profiles with matrix weights **A** and (**I−A**), respectively. In equation (8) the contribution of the a priori profile element at level i to one retrieved profile element at level z is assumed to have a weight of $(I(z, z_i) - A_{fr}(z, z_i))$ on a total of $(A_{fr}(z, z_i) + I(z, z_i)) - A_{fr}(z, z_i))$; the total weight to one retrieved element is then given by the summation over all levels i. Equation (8) has been applied to calculate the a priori fractions of the five OE-based algorithms and the results are shown in Figures 5a and 5b.

[58] Related to the a priori fraction is the quantity called degrees of freedom for the signal (DFS), which is defined as the trace of **A** (i.e., ΣA_{ii}, following *Rodgers* [2000, p. 37]). The median and the standard deviation of the DFS values have been printed in each plot of Figures 5a and 5b.

3.6. Conclusions for Interpretation of OE and PTR Retrieved Data

[59] On the basis of the results presented in Figures 3a, 3b, 4a, 4b, 5a and 5b, we can now draw conclusions on how to interpret the results of those retrieval algorithms delivering data including averaging kernels and (if applicable) a priori information. In the estimation of the vertical resolution the presented results are in the range 9–13 km for the OE-based algorithms and for the PTR-based algorithm, over a limited (between 12 and 32–36 km) altitude range, about 8 km. The altitude range with better than 15 km resolution for the OE methods generally starts at 16–18 km, with some exceptions in the polar regions of 22–25 km (i.e., KNMI, RAL, and SAO algorithms), and ends at 38–47 km. The lowest altitude is correlated to an altitude in between the local tropopause and the local ozone maximum, i.e., in the middle of the lower stratosphere. If wavelengths below 290 nm are not used, then a much lower resolution is found in the altitude range 40–50 km (i.e., IUP, SAO and SRON algorithms). Some other striking features appearing from this overview are the extent to lower altitudes of the SRON algorithm, the small range with worse resolution around 25- to 28-km altitude (apparent in some regions for IUP, KNMI and NOAA),

length) for the OE methods. Second, there is a bias toward the a priori profile used in the OE retrievals, which occurs when there is not enough measurement information. The first term has already been dealt with in section 3.3, and

and the different results, especially in the polar regions, of IUP compared to the other OE-based algorithms.

[60] The centroid of the averaging kernel is the second interpretation parameter that we have investigated. We will now analyze the results of the derived centroids by examining over which altitude range the centroids do not deviate more than 4 km from their nominal altitude (i.e., within diagonal dotted lines in Figures 4a and 4b). The bottom altitude of this valid range is around 9–12 km in the polar regions, about 16 km at midlatitudes and about 19 km in the tropics. The valid range for this parameter is also limited at the upper altitude by the lack of exploiting the GOME data with wavelengths below 290 nm, which then decreases from 48–50 km to 39–44 km. The RAL retrieval uses larger than climatological a priori values in the troposphere and this, in itself, may induce the deviation of the centroids below the nominal altitude of 25 km, but on the other hand this is the only retrieval algorithm giving some "valid" centroid values (i.e., within 4 km of their nominal altitude) lower than 10 km. This is assumed to be due to fitting the temperature-dependent structure in the Huggins ozone bands to higher precision than the other algorithms in combination with the assumption of a relatively large a priori error (100%) in the troposphere. In general the lowest median centroid values range from 14 km in the polar regions to 19 km at midlatitudes and in the tropics, with the remarkable exception of 8 km for the RAL retrieval in the tropical region.

[61] The third interpretation parameter that we have presented is the a priori fraction. The derived values for this parameter would be close to zero in the ideal case, and the values go to one in the case that the retrieval does not exploit the measurement information in the spectra and relies completely on the a priori. We have derived over which altitude range the a priori fractions are smaller than 0.33, which we still regarded to be an acceptable fraction (nevertheless, retrievals with larger a priori fractions are of value, provided that this is recognized and accounted for by the data user). In general this requirement is met between about 8- and 48-km altitude. However, there are some exceptions and special features, e.g., the KNMI, RAL and SAO results show larger than 0.33 negative values between about 11 and 18 km altitude in the tropical and midlatitude regions. In the IUP retrieval all the information is retrieved from just below the tropopause up to about 41-km altitude, and the upper limit is again likely to be correlated to the lack of using the shortest wavelengths. However, this is not visible in the SAO results which are also not using the wavelengths below 290 nm, because it uses large a priori errors above 40 km. Furthermore, it is quite remarkable that although the NOAA retrieval only uses parts of the complete GOME spectra, its results compared to the other retrievals indicate that this algorithm has acceptable fractions over nearly the entire altitude range, which is probably also here the result of using larger a priori errors in the retrieval. Finally, the retrieved data from the RAL algorithm also indicate to sometimes contain (acceptable) tropospheric information below 8-km altitude, with the exception of Andoya in the arctic region.

[62] In Figures 5a and 5b we have also provided the DFS, and when decomposed per altitude level (not shown), this parameter shows that almost all ozone information present in the GOME data is retrieved as stratospheric information, which is true for almost all the global regions and for all algorithms. In total there are only four to six independent pieces of information, or DFS, allowing the retrieval of (possibly) one point in the troposphere and maximum five to six points in the stratosphere.

3.7. Effect of Averaging Kernel Representation

[63] The preceding analysis was based on kernels which were scaled with the a priori ozone values, resulting in fractional kernels. The derived measures of vertical resolution and indicative altitude can only be interpreted straightforwardly if relative perturbations of similar magnitude can be expected at all the altitudes to which a particular retrieved value is sensitive. As might be expected, the kernels indicate that retrieval for levels below the ozone peak are strongly sensitive to perturbations in ozone peak concentration, since at this altitude a given fractional perturbation has most impact on the measurements. However, in reality (according to the *Fortuin and Kelder* [1998] climatology), ozone concentrations at and above the ozone peak vary relatively little compared to those in the troposphere and lower stratosphere. The expected perturbations in this altitude range in, for example, the subtropics in April (from the Fortuin and Kelder climatology), are more constant with altitude when expressed in absolute (i.e., number density) rather than in fractional changes. This statistical representation of the climatological variation of ozone is represented in the a priori used in a number of the OE schemes described here. For these lower altitude levels, it is therefore often the case that figures of merit derived from number density averaging kernels provide more insight into the true performance of the retrieval scheme. The sensitivity of tropospheric and lower stratospheric levels to higher-level perturbations will degrade the corresponding estimates of vertical resolution and indicative altitude derived for these lower altitude levels. However, the sensitivity to nonlocal perturbations is only important if, in reality, such perturbations actually occur with relative magnitude similar to their local concentrations.

[64] When assuming equal amplitude perturbations in terms of number density, rather than in fractional units, the interpretation of the corresponding averaging kernels changes. It results in different resolving lengths, centroids and fractions of a priori information. To demonstrate this difference for the retrieval levels below 20-km altitude, the centroids and resolving lengths have also been computed for the averaging kernels assuming equal number density perturbations. For these kernels the response to the true profile has been cut off at 26-km altitude because above this altitude such a representation is highly unlikely. The alternative results are shown in Figures 3a, 3b, 4a and 4b, with the thick gray lines. As the alternative results for the fractions of a priori information are quite similar to those using fractional kernels, these results have not been plotted in Figures 5a and 5b.

[65] The conclusions in section 3.6 about the useful altitude range are dependent on the averaging kernel representation used in the analysis. In general, this alternative interpretation gives better resolving lengths below 20-km altitude with typical values of 15 km, and centroids indicating that the retrieval system can also have sensitivity in

Table 3. Errors (Systematic and Random) Expected Within Ozone Lidar Data of the NDSC[a]

Altitude Range, km	Accuracy,%	Precision,%
<20	5–10 without Raman channels[b]	5
<20	5 with Raman channels[b]	5
20–35	2	2
>35	5–10	5–10

[a]From *Keckhut et al.* [2004, Table 3].
[b]See Table 2 for which systems have Raman channels.

the lower atmosphere. For example, in this representation RAL centroids already lie within 4 km of the nominal retrieval altitude from the midtroposphere instead of 20-km altitude previously. The dependence of the figures of merit on the unit of perturbation highlights the fact that the sensitivity to the lower atmosphere is mediated by the true anomaly in the middle (and higher) atmosphere. Therefore the correct representation and interpretation depends on the true situation or at least a realistic expected variation, which is in addition dependent on season and global region.

4. Intercomparison With Lidar Data

4.1. Introduction

[66] For the comparison to GOME ozone profiles, we use correlative data from the Network for Detection of Stratospheric Change (NDSC) stations for the years 1997–1999. We incorporate lidar data measured at Andoya in Norway, Observatoire Haute Provence (OHP) in France, Mauna Loa Observatory (MLO) on Hawaii, Lauder in New Zealand, and Dumont d'Urville on Antarctica (see Table 2), which allows the analysis of GOME data measured in different global regions, including polar, midlatitude and tropical cases. The aim of this section is to assess the quality of the GOME ozone profiles in these regions, which have different atmospheric characteristics and represent different viewing geometries of GOME. As GOME is in a Sun-synchronous orbit (with an overpass in the late morning (local time)), the observations at low latitudes are on average with small solar zenith angles and the reverse holds for high latitudes (i.e., generally large solar zenith angles).

4.2. Stratospheric Ozone Lidar Data

4.2.1. Lidar System Description

[67] Stratospheric ozone lidar systems measure the atmosphere between about 10- and 50-km altitude. These measurements are performed between 1 and 3 times per week, depending on weather and atmospheric conditions. Lidar systems are usually operated at night, but some lidars have been adapted for daytime use in polar regions. Stratospheric ozone lidar instruments use a special lidar system which is called a differential absorption lidar (DIAL) system [*Measures*, 1984; *McDermid et al.*, 1990]. These systems simultaneously emit two light pulses at different wavelengths with different ozone absorption cross sections. The ratios in light intensity backscattered from different altitudes can be directly related to the local ozone concentrations. Data are provided as ozone number densities as a function of geometric altitude.

4.2.2. Lidar Data Quality

[68] Validation of data implicitly means the use of reliable correlative data with known (high) quality for the analysis.

The correlative data used in this study come from stations that are part of the NDSC. The initiative for this network [*Network for Detection of Stratospheric Change*, 1986] http://www.ndsc.ws) was based on the need for such worldwide high-quality measurements, among others for validation of satellite-based sensors. The NDSC comprises a number of ground-based measurement stations employing the full suite of instruments and located at strategic positions on the globe. They are supplemented with measurements performed at complementary stations (see Table 2). The NDSC measurements are regularly monitored for their quality via measurement validation campaigns performed under the NDSC protocol. For the lidars considered here, see the following references for the papers about the MLO95 [*McPeters et al.*, 1999], OPAL [*McDermid et al.*, 1998a, 1998b], and OHP97 (G. O. Braathen et al., Intercomparison of stratospheric ozone and temperature measurements at the Observatoire de Haute Provence during an NDSC validation campaign from 1–18 July 1997, manuscript in preparation, 2006) campaigns at the Mauna Loa, Lauder, and OHP NDSC stations, respectively. In addition, *Keckhut et al.* [2004] recently published a review paper of all these activities, and their general conclusion on the lidar data quality is provided in Table 3.

4.2.3. Collocation Criteria

[69] The ozone profiles, from the lidar stations mentioned above, will be used for comparison to GOME ozone profiles. As the lidar instruments did not exactly sample the same atmosphere as the satellite instrument, we will need to define criteria which allow a certain (maximum) difference in both location and time between the two observations. In the GOME1-O3P-WG it was agreed to use windows of 12 hours and 500 km for the allowed temporal and spatial differences, respectively, which in the case of coadding of pixels resulted in a maximum distance of 800 km. Previous studies [*Veiga et al.*, 1995; *Meijer et al.*, 2003, 2004] demonstrated that a 20-hour time window and a circle with an 800-km radius were already appropriate collocation criteria, for SAGE I/II, GOME, and GOMOS satellite data, respectively. *Meijer et al.* [2004] demonstrated in a separate analysis that with stricter collocation criteria (10 hours and 400 km, respectively), which are then very similar to those used here, the standard deviation of the differences can generally be within 10–13% (20–50 km) and within 15% down to 17-km altitude. *Brinksma et al.* [2000] showed that allowing a time difference of up to 24 hours, the standard deviation of the differences between collocated lidar and sonde observations remained small down to 10-km altitude. Furthermore, we required that a lidar measurement can only be paired once with GOME data (i.e., data sets are bijective).

4.3. Comparison Approach

[70] In the GOME1-O3P-WG it was agreed to report all data as ozone number density versus geometric altitude with fixed 2-km intervals. However, the comparison of different data sets also raises other issues about their comparability. One of the most important issues is how to deal with differences in vertical resolution. For the comparison to the GOME data that come with averaging kernels and (if applicable) a priori information, we have

transformed the lidar data by substituting the lidar profile for the vector $\mathbf{x_{true}}$ in equation (1). This approach was first suggested by *Connor et al.* [1991]. For the averaging kernel values outside the lidar altitude range, the lidar profiles are completed with the global ozone climatology of *Fortuin and Kelder* [1998]. The "lidar profile" resulting from equation (1) is now referred to as "transformed" lidar data and compared to the GOME retrieved data. These transformed lidar data are no longer completely independent from the GOME data [*Meijer et al.*, 2003], and comparison results should never be regarded without the interpretation results of section 3, e.g., the analysis method may give the appearance of good performance in regions where an algorithm returns the a priori. For the GOME retrievals using the NN and DA approaches, their data are compared to the lidar data integrated on a 2-km altitude grid, which hereafter are referred to as "regridded" lidar data.

[71] An example of the retrieved data sets, collocated with Lauder (New Zealand), is shown in Figures 2c and 2d, in which Figure 2d is used to illustrate the spread in the retrieved data obtained from the same spectral information. It is important to note that the intercomparison results of the OE- and PTR-based algorithms cannot be directly compared to the results of the NN- and DA-based algorithms, because the comparisons involve transformed and regridded lidar data, respectively, which typically differ in vertical resolution by a factor of two (or more). For example, the steep gradient in the ozone concentrations of the lower stratosphere will have a smaller impact on the comparison results involving transformed lidar data.

[72] From the set of collocated pairs we calculate the median of their differences; with differences calculated as GOME minus (transformed or regridded) lidar data in percentage relative to the latter. We choose to calculate the median rather than the mean, which was done to avoid possible disturbance in the results coming from outliers. In addition the standard deviation of these relative differences (hereinafter referred to as STD) is calculated according to

$$\mathrm{STD}(z) = \sqrt{\frac{1}{N-1} \sum_{j=1}^{N} \left(d_j(z) - \overline{d}(z)\right)^2}, \qquad (9)$$

where d_j is the relative difference in percentage of (GOME$_j$ − lidar$_j$)/lidar$_j$, $\overline{d}$ is the mean of these differences, and N is the number of pairs.

4.4. Results per Geolocation

[73] The intercomparison results for the five OE-based algorithms are shown in Figure 6a (IUP, KNMI, and RAL) and Figure 6b (left and middle) (SAO and NOAA). The results of the PTR-based algorithm are shown Figure 6b (right) (SRON). The two NN-based algorithms are shown in Figure 6c (left and middle) (UTV and ZSW) and Figure 6c (right) contains the results of the DA-based algorithm (DLR). Each row in Figures 6a–6c represents the results coincident with a certain lidar station, which ranges from the Arctic (Figures 6a–6c, top) to the Antarctic (Figures 6a–6c, bottom) in order of latitude. In Figures 6a–6c we have also indicated the actual number of intercomparison pairs,

and hence this shows the number of successfully realized retrievals.

4.5. Conclusions of Intercomparison Results

[74] The intercomparison results of the IUP, NOAA, and KNMI retrievals demonstrate qualitatively similar oscillations in the derived biases (in particular see the OHP, MLO and Lauder median results), but for KNMI the shape is less pronounced. RAL, on the other hand, has results with opposite features and SAO does not demonstrate any such oscillations. As the NOAA algorithm is not a GOME "native" algorithm (i.e., its algorithm was designed for SBUV data), this algorithm completely relies on well-calibrated spectra. Therefore its relatively worse results are not entirely unexpected, because we have seen in section 2 that in the other algorithms a substantial effort has been put in optimizing their input spectra. Both the IUP and the NOAA algorithm have used a relatively large a priori error (30% and 50%, respectively) in the retrieval allowing more freedom to the system to extract more data from the measurement, but too large errors will introduce noise rather than more information which seems to be the case. The SAO and SRON algorithms have little in common, apart from the exploited wavelength range, nevertheless, their derived biases are rather similar and generally show a positive bias at low altitudes linearly changing to a negative bias higher up. A possible explanation can be that both algorithms do not apply a wavelength-dependent correction to the GOME spectra at the shortest wavelengths.

[75] The data quality of the NN-based algorithms cannot be better than the quality of their training data set. In almost all cases the STD involving UTV data are larger than the STD involving RAL data, which was its training set. In general the features of the RAL and UTV biases are quite similar, but certainly not in all regions and this might be caused by the fact that an older version of the RAL data was used in the training. The intercomparison results of the ZSW algorithm show a small (∼5% positive or negative) bias close to zero, with a STD of 5%, 5−10%, and 10% for the results in tropical, midlatitude and polar regions, respectively. The results of the UTV algorithm are qualitatively quite similar to the results of the ZSW algorithm, but the STD is generally 1.5 times larger. The altitude range with a relatively low STD is approximately 17−44 km for both NN-based algorithms. For the DA-based retrieval we found intercomparison results with generally a larger STD (about 15%) compared to the other approaches. The altitude range with relatively low STD is 15−45 km, and here the bias is negative (15%) at lower and positive (15%) at higher altitudes. The bias of this algorithm in the Arctic region is quite small, but with a large STD. Note that the DA algorithm only uses total column information from GOME and obtains the profile shape from the model.

5. Discussion

[76] The aim of this paper was to evaluate the nine different GOME ozone profile retrieval algorithms that are currently available. We gave an overview of four different approaches, and briefly described their characteristics and way of implementation into a retrieval algorithm. We have confronted these algorithms with the same set of GOME
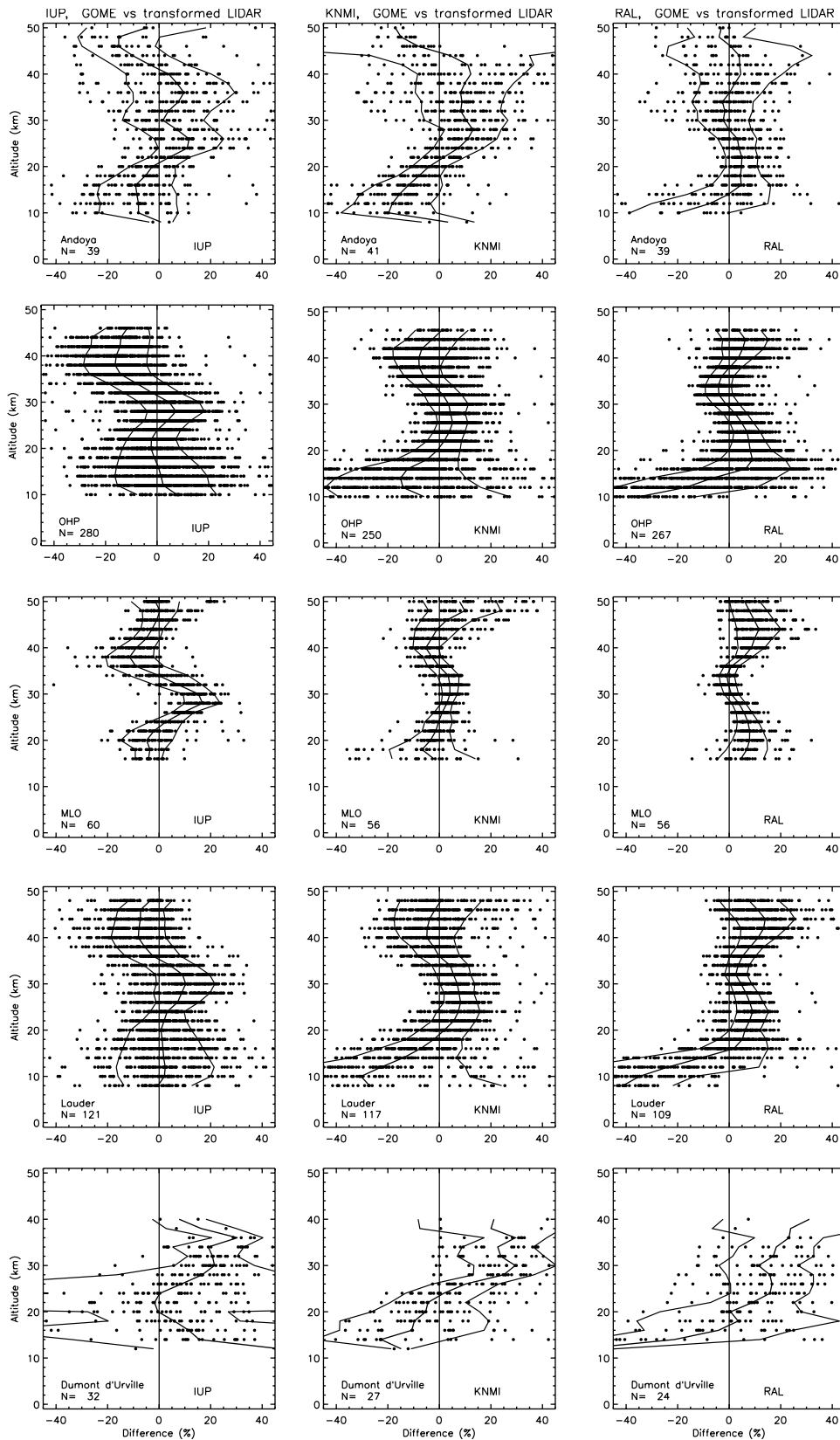
Figure 6a. Individual intercomparison results (dots) of three GOME retrievals collocated with lidar measurements near the NDSC stations at Andoya, OHP, MLO, Lauder, and Dumont d'Urville, shown from the top downward ranging from north to south, respectively. Differences are calculated as GOME minus (transformed or regridded) lidar data in percentage relative to the latter. Median (thick line) and standard deviation (thin line) of the relative differences are also shown.
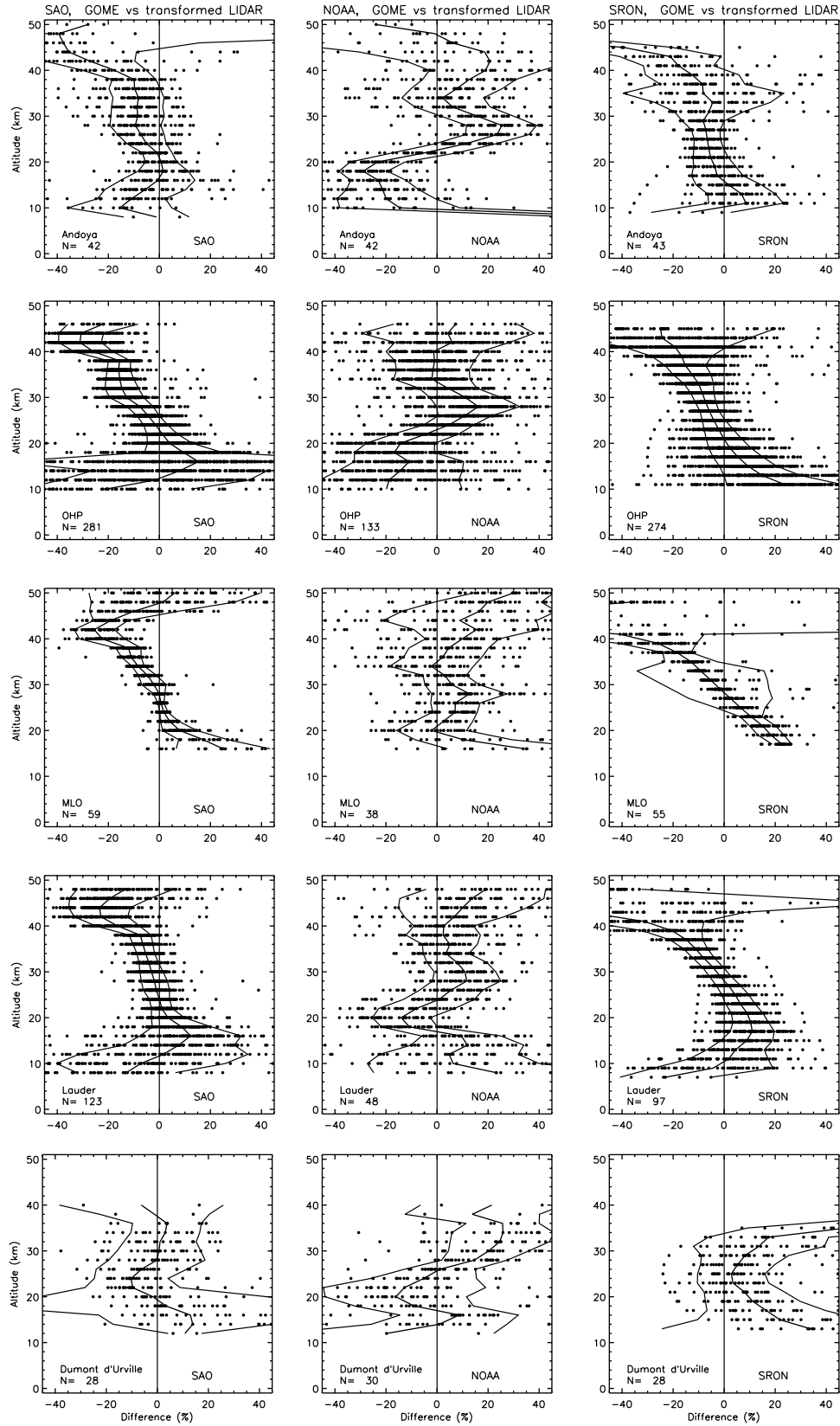
Figure 6b. Same as Figure 6a, but now showing the results for three other algorithms.
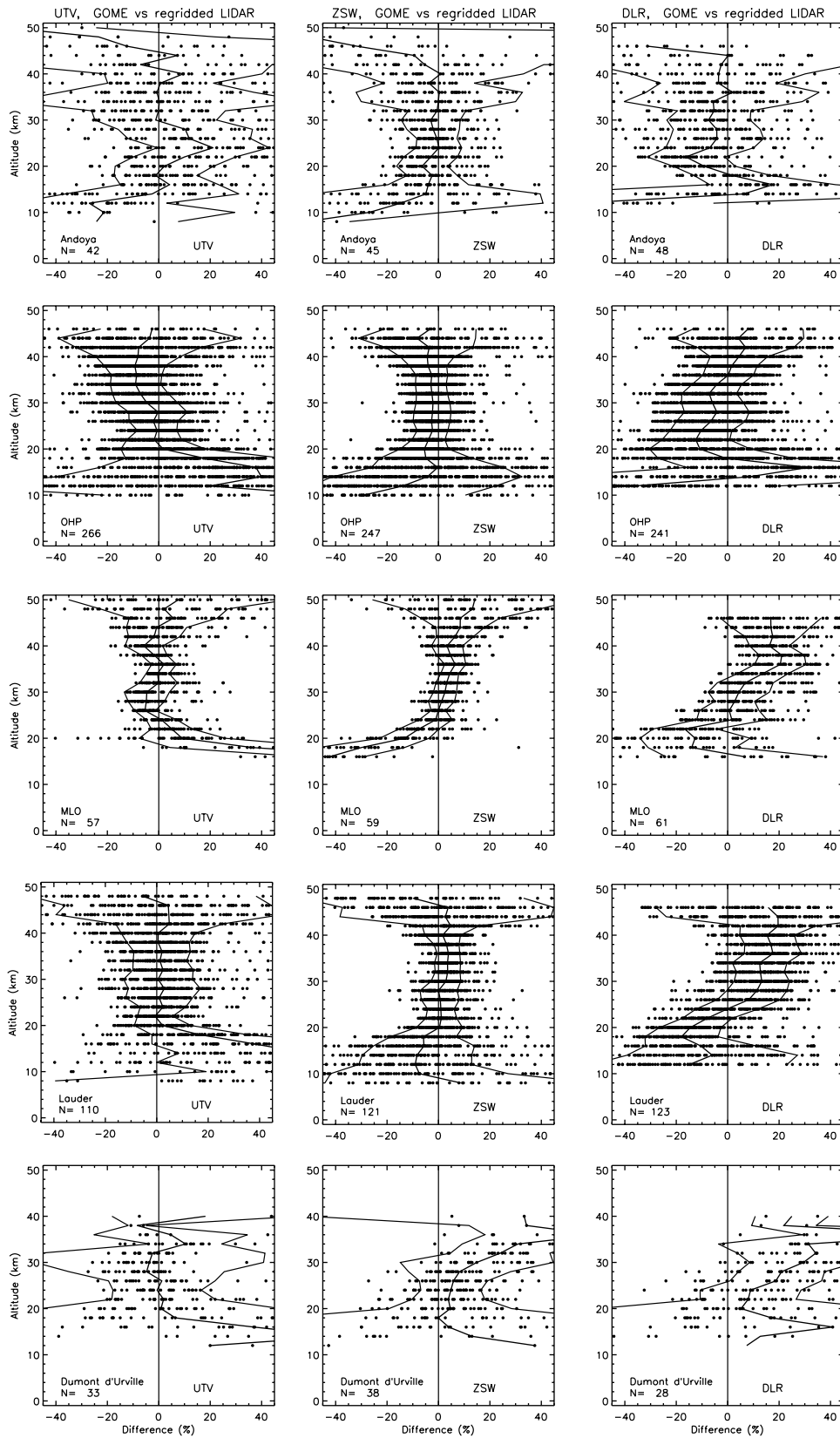
Figure 6c. Same as Figure 6a, but now showing the results for three other algorithms.
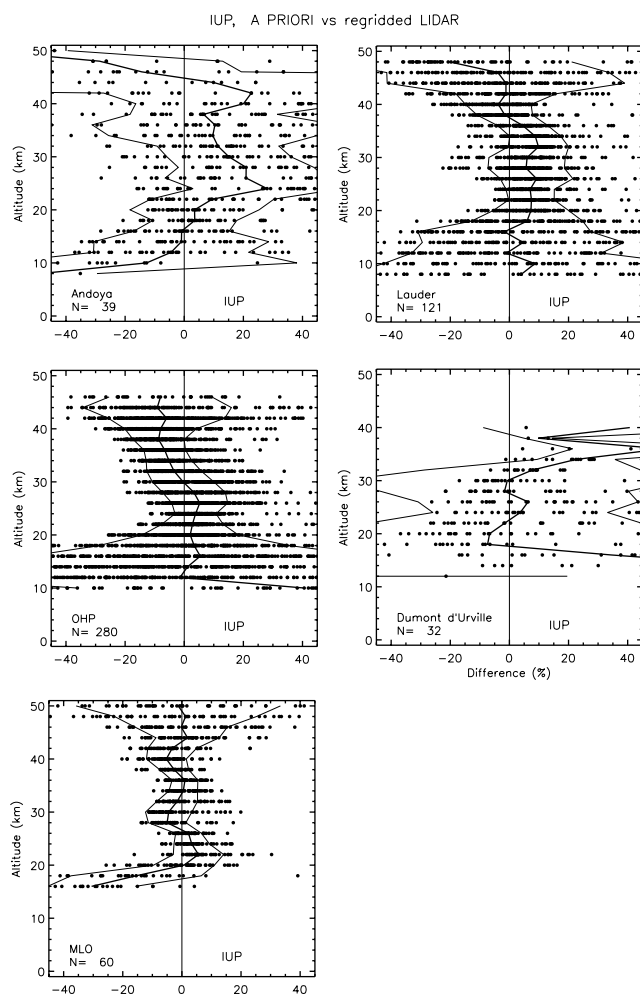
Figure 7. Same as Figure 6a, but now showing intercomparison results of climatological data, which are used in some retrievals, compared to lidar data measured at the NDSC stations of Andoya, OHP, MLO, Lauder, and Dumont d'Urville, shown from the top downward and from left to right ranging from north to south, respectively.

spectra, analyzed their response, and compared results to high-quality ground-based measurements to assess their quality. For the retrievals that provide averaging kernels and (if applicable) use a priori information, we have applied interpretation tools. These tools provide figures of merit for the retrieved product regarding the vertical resolution, the actual retrieval altitude and the reliance on a priori information. Here the comparison results should never be regarded without these interpretation results, because the applied comparison method gives the appearance of good performance, compared to the transformed lidar data, in situations where an algorithm basically returns the a priori.

[77] For the OE- and PTR-based algorithms, we can derive the valid and acceptable altitude range of the retrieved data from the interpretation results based on quantitative requirements, here assumed to be that the fractional averaging kernels have a resolution estimate lower than 15 km, a centroid that is within 4 km of its nominal altitude and an a priori fraction smaller than 0.33. The last requirement is not applicable to the PTR-based approach. On the

basis of these requirements, the valid and acceptable altitude range is 15–48 km in which the data have an average resolution of 10 to 15 km. The upper altitude of the range is determined by whether the shortest wavelengths are taken into account. Because the ozone absorption cross section increases below 270 nm, these channels are needed to retrieve ozone at the higher altitudes where the ozone density is dropping off rapidly. However, the limitation in using shorter wavelength is the increasing measurement error, and currently the highest altitude is 48 km.

[78] The lower boundary of the acceptable range is mainly related to the altitude at which the ozone concentrations are too low, compared to the values at higher altitudes, such that, if altitude-independent relative changes in ozone are assumed, the signal from higher-altitude dominates the retrieval. This generally occurs in the middle of the (local) lower stratosphere. It is important to note that the estimate for the lower limit is dependent on the representation of the averaging kernels that have been analyzed (see section 3.7). If number density kernels are analyzed for the lower retrieval levels, rather than fractional kernels, then the valid and acceptable altitude range extends downward, which in some cases even reaches down into the midtroposphere.

[79] For the NN-based algorithms, it is more difficult to draw similar conclusions, especially as averaging kernels were not available and therefore it is not explicitly clear where the retrieved profile information came from. However, it is possible to derive a valid range by analyzing their results in the intercomparison with the lidar data. When assuming that the NN algorithm found the perfect statistical link between the profile information in the spectra and the collocated ("true") ozone profile used in the training, then the altitude regions with a small STD in the intercomparison with lidar reflect the presence of profile information in the GOME measurements. The NN algorithms have this small STD in the altitude range 17–44 km, and this is almost exactly the same range as obtained with the OE and PTR algorithms. Though it should be noted that the 2-km interpolated grid is ambitiously fine and may have led to an underestimate of retrieval quality in the lower stratosphere, where fine vertical structure is particularly present in the lidar data which is unlikely to be resolved by GOME.

[80] For the DA-based algorithm, the interpretation can also be done by looking at the altitude region in which the STD is small in the comparison results with lidar data. The DA-based algorithm has this small STD in the altitude range 15–45 km, but it should be noted that its STD is generally larger than those from the other schemes. The higher STD is possibly due to the relatively coarse horizontal model resolution compared to the GOME resolution. A significant improvement in the 3-D ozone analysis is expected when ozone profiles, derived by an OE, PTR or NN approach, are assimilated in the model, instead of ozone columns.

[81] In the derived valid altitude range we can potentially expect the retrieved data to be acceptable. The next step is to assess its quality, but before doing so we initially look at what we already knew, and in Figure 7 we show the comparison results of the regridded lidar data compared to the climatology used by IUP (and KNMI and RAL). It demonstrates the prior knowledge we had regarding bias and variance compared to the "true" profile, but note that

this is a comparison based on a higher resolution than the intercomparison of the retrieved GOME data with the transformed lidar data. From Figure 7 it becomes clear that some of the features in the observed biases are introduced by errors in the GOME level 1 data or the forward model used by the retrieval algorithms, as they were neither present in the a priori comparison nor in the intercomparison results of the NNs. As mentioned in section 4.5, this problem is likely to be related to the inadequate calibration accuracy, as for ozone profile retrieval from nadir UV spectra a high accuracy is required.

[82] The intercomparison results with lidar data demonstrated that the retrieved data have a precision of 5–10% and a bias up to 5% or 20% depending on the success of recalibration of the input spectra for the physical approaches and depending on the training data set for the NN-based algorithms. The NN approach has the advantage that the retrieval does not rely on well-calibrated GOME spectral data, and instead it relies on the high quality of the data used in the training process. This advantage is however lost in the case of the UTV algorithm, since this algorithm used RAL data for the training, which requires the calibration accuracy. Nevertheless, the limited exploited spectral range by the UTV algorithm might cause it to just return an average representative RAL profile. Furthermore, from the results presented in this paper it, too, became clear that OE-based algorithms strongly depend on the a priori ozone profile information, and its error covariance matrix, used in the retrieval. In the OE approach these a priori quantities should be carefully chosen, and should be regarded as a "fixed" or known atmospheric property [see also *Rodgers*, 2000, chapter 10]. Although some groups indeed use similar climatologies, they are not the same over the whole atmosphere and the choices applied for the covariance matrix are also different (i.e., variance and correlation length). Both settings have their implications for the retrieved ozone profile and its corresponding averaging kernel matrix.

6. Conclusions and Future Work

[83] In 2003, after the discontinuation of the GOME1-O3P-WG, ESA initiated an invitation to tender and finally funded a 2-year project called CHEOPS-GOME, which aims to exploit GOME measurements for the provision of ozone profiles. Within this project two different ozone profile climatologies will be set up and provided to a broad user community in atmospheric science. First, there will be a common climatology generated as a look-up table in ASCII format. Second, a climatology based on the NN technique will be built, which should be more flexible concerning temporal and spatial resolution. Also additional parameters (e.g., total ozone column, temperature profile) and other optional user specifications can be considered with a NN-based climatology. Furthermore, a more accurate prototype algorithm, based on the OE technique, shall be developed for future implementation into an operational processor, which will then be used to process the data of the complete 8-year GOME mission. This work includes the development of a new (improved) spectral calibration algorithm to ensure high-accuracy ozone profile retrieval. Data from the currently operational algorithms, presented in this paper, are available on request. A major processing of

the full mission is underway using the RAL algorithm, which will be made available through the British Atmospheric Data Centre (BADC, http://badc.nerc.ac.uk/data/gome).

[84] The general conclusion of this paper is that ozone profile information can be retrieved from GOME spectra, with low a priori contribution, in the altitude range 15–48 km with a vertical resolution of 10 to 15 km. Outside this altitude range, more care needs to be taken to interpret retrievals using the full averaging kernel matrix. Direct, robust determination of tropospheric ozone, with minimal a priori contribution, has not been demonstrated in this study. Nevertheless, analysis of averaging kernels indicates sensitivity to tropospheric ozone in a number of schemes, and a tropospheric layer number density can be recovered by optimal estimation, provided that the true variation of stratospheric ozone conforms to the assumed a priori variability. In general, the GOME ozone profile data have a precision of 5–10% and a bias up to 5% or 20%. In addition, the GOME data, for the OE methods, allow the retrieval on about six independent altitude levels without adding too much a priori information.

[85] The conclusions and limitations presented here are partly driven by physical limitations of the nadir UV measurement approach for ozone profiling. In general similar results can be expected for similar retrieval schemes applied to other moderate resolution, nadir-viewing observations of instruments like SCIAMACHY, OMI and GOME-2. It should however be noted that this analysis is limited to the particular profile retrieval schemes which have been investigated, each of which seeks to cope with deficiencies in the GOME level 1 data. The inherent information content of UV spectra for profile retrieval, particularly with respect to the lower atmosphere has not yet been fully exploited by any scheme to date. It is expected that, because experience from GOME(-1) has fed into the instrument design and preflight characterization, new instruments like OMI and GOME-2 will provide more accurate and potentially better resolved measurements of the ozone profile. In particular it was noted in the GOME-2 error study [*Kerridge et al.*, 2003] that insufficient knowledge of the instrument spectral response (slit) function shape was a major limiting factor for tropospheric retrieval from GOME-1. Both OMI and GOME-2 will be far better characterized in this respect.

[86] Exploitation of the tropospheric sensitivity from nadir-viewing measurements in the UV-visible is a rapidly evolving field of study. The ozone profile retrieval below 15-km altitude can also be expected to improve when additional tropospheric information is used, such as exploiting polarization effects [*Hasekamp and Landgraf*, 2002b], which will be possible for GOME-2. Upper tropospheric and stratospheric observations by limb sounders, such as MIPAS on Envisat and MLS on EOS-Aura, may also help to constrain retrievals leading to better tropospheric products. Nearby measurements made in both the presence and absence of clouds can also be used to provide information on the subcolumn of ozone obscured by the cloud. The ability to adequately characterize scattering and absorption by cloud and aerosol will be crucial if the information content of any of these measurement techniques is to be usefully exploited.

References

Ahmad, Z., and P. K. Bhartia (1995), Effect of molecular anisotropy on the backscattered UV radiance, *Appl. Opt.*, *34*, 8309–8314.

Anderson, G., S. Clough, F. Kneizys, J. Chetwynd, and E. Shettle (1986), AFGL atmospheric constituent profiles, *Tech. Rep. AFGL-TR-86-0110*, Air Force Geophys. Lab., Bedford, Mass.

Bass, A. M., and R. J. Paur (1984), The ultraviolet cross-sections of ozone: I. The measurements of atmospheric ozone, in *Proceedings of the Quadrennial Ozone Symposium*, pp. 606–610, Springer, New York.

Bauman, J. J., P. B. Russell, M. A. Geller, and P. Hamill (2003), A stratospheric aerosol climatology from SAGE II and CLAES measurements: 1. Methodology, *J. Geophys. Res.*, *108*(D13), 4382, doi:10.1029/2002JD002992.

Bhartia, P. K., (Ed.) (2002), *OMI Algorithm Theoretical Basis Document*, vol. 2, *OMI Ozone Products*, NASA Goddard Space Flight Center, Greenbelt, Md.

Bhartia, P. K., and C. G. Wellemeyer (2002), *OMI Algorithm Theoretical Basis Document*, vol. 1, *TOMS-V8 Total Ozone Algorithm*, edited by P. K. Bhartia, NASA Goddard Space Flight Center, Greenbelt, Md.

Bhartia, P. K., R. D. McPeters, C. L. Mateer, L. E. Flynn, and C. Wellemeyer (1996), Algorithm for the estimation of vertical ozone profiles from the backscattered ultraviolet technique, *J. Geophys. Res.*, *101*, 18,793–18,806.

Bishop, C. M. (1995), *Neural Networks for Pattern Recognition*, Clarendon, Oxford, U. K.

Boersma, K. F., H. J. Eskes, and E. J. Brinksma (2004), Error analysis for tropospheric NO2 retrieval from space, *J. Geophys. Res.*, *109*, D04311, doi:10.1029/2003JD003962.

Brinksma, E. J., et al. (2000), Validation of 3 years of ozone measurements over Network for the Detection of Stratospheric Change station Lauder, New Zealand, *J. Geophys. Res.*, *105*, 17,291–17,306.

Burrows, J. P., et al. (1999a), The Global Ozone Monitoring Experiment (GOME): Mission concept and first scientific results, *J. Atmos. Sci.*, *56*, 151–175.

Burrows, J. P., et al. (1999b), Atmospheric remote-sensing reference data from GOME: 2. Temperature-dependent absorption cross sections of O₃ in the 231–794 nm range, *J. Quant. Spectrosc. Radiat. Transfer*, *61*, 509–517.

Caudill, T. R., D. E. Flittner, B. M. Herman, O. Torres, and R. D. McPeters (1997), Evaluation of the pseudo-spherical approximation for backscattered ultraviolet radiances and ozone retrieval, *J. Geophys. Res.*, *102*, 3881–3890.

Chance, K. V., and R. J. D. Spurr (1997), Ring effect studies: Rayleigh scattering, including molecular parameters for rotational Raman scattering, and the Fraunhofer spectrum, *Appl. Opt.*, *36*, 5224–5230.

Chance, K., T. P. Kurosu, and C. E. Sioris (2005), Undersampling correction for array detector based satellite spectrometers, *Appl. Opt.*, *44*, 1296–1304.

Chin, M., P. Ginoux, S. Kinne, O. Torres, B. Holben, B. N. Duncan, R. V. Martin, J. A. Logan, A. Higurashi, and T. Nakajima (2002), Tropospheric aerosol optical thickness from the GOCART model and comparisons with satellite and sunphotometer measurements, *J. Atmos. Sci.*, *59*, 461–483.

Connor, B. J., A. Parrish, and J.-J. Tsou (1991), Detection of stratospheric ozone trends by ground-based microwave observations, *Proc. SPIE Int. Soc. Opt. Eng.*, *1491*, 218–230.

Connor, B. J., A. Parrish, J.-J. Tsou, and M. P. McCormick (1995), Error analysis for the ground-based microwave ozone measurements during STOIC, *J. Geophys. Res.*, *100*, 9283–9291.

Daily, R. (1991), *Atmospheric Data Analysis*, 457 pp., Cambridge Univ. Press, New York.

Dave, J. V. (1964), Meaning of successive iteration of the auxiliary equation of radiative transfer, *Astrophys. J.*, *140*, 1292–1303.

Del Frate, F., A. Ortenzi, S. Casadio, and C. Zehner (2002), Application of neural algorithms for a real-time estimation of ozone profiles from GOME measurements, *IEEE Trans. Geosci. Remote Sens.*, *40*, 2263–2270.

Deutsches Zentrum für Luft- und Raumfahrt (1996), GOME level 0 to 1 algorithms description, *Tech. Note ER-TN-DLR-GO-0022*, Oberpfaffenhofen, Germany.

Fortuin, J. P. F., and H. Kelder (1998), An ozone climatology based on ozonesonde and satellite measurements, *J. Geophys. Res.*, *103*, 31,709–31,734.

Hansen, P. C. (1994), Regularization tools—A Matlab package for analysis and solution of discrete ill-posed problems, *Numer. Algorithms*, *6*, 1–35.

Hansen, P. C., and D. P. O'Leary (1993), The use of the L-curve in the regularization of discrete ill posed problems, *SIAM J. Sci. Comput.*, *14*, 1487–1503.

Hare, E. W., E. J. Carty, and V. E. Fioletov (2004), Recent advancements and challenges at the WOUDC from a historical perspective, paper presented at the Quadriennial Ozone Symposium, Int. Assoc. for Meteorol. and Atmos. Sci., Kos, Greece, 1–8 June.

Hasekamp, O. P., and J. Landgraf (2001), Ozone profile retrieval from backscattered ultraviolet radiances: The inverse problem solved by regularization, *J. Geophys. Res.*, *106*, 8077–8088.

Hasekamp, O. P., and J. Landgraf (2002a), A linearized vector radiative transfer model for atmospheric trace gas retrieval, *J. Quant. Spectrosc. Radiat. Transfer*, *75*, 221–238.

Hasekamp, O. P., and J. Landgraf (2002b), Tropospheric ozone information from satellite-based polarization measurements, *J. Geophys. Res.*, *107*(D17), 4326, doi:10.1029/2001JD001346.

Hasekamp, O. P., J. Landgraf, and R. van Oss (2002), The need of polarization modeling for ozone profile retrieval from backscattered sunlight, *J. Geophys. Res.*, *107*(D23), 4692, doi:10.1029/2002JD002387.

Hilsenrath, E., J. Gleason, S. Janz, X. Gu, R. P. Cebula, K. Chance, and R. Hoekstra (1996), GOME calibration and validation using backscatter UV techniques, in *Proceedings of the GOME Geophysical Validation Campaign Workshop (Frascati, Italy, 24–26 January 1996)*, *Rep. WPP-108*, p. 85, Eur. Space Agency, Paris.

Hoogen, R., V. V. Rozanov, and J. P. Burrows (1999), Ozone profiles from GOME satellite data: Algorithm description and first validation, *J. Geophys. Res.*, *104*, 8263–8280.

Joiner, J., P. K. Bhartia, R. P. Cebula, E. Hilsenrath, R. D. McPeters, and H. W. Park (1995), Rotational-Raman scattering (ring effect) in satellite backscatter ultraviolet measurements, *Appl. Opt.*, *34*, 4513–4525.

Keckhut, P., et al. (2004), Review of ozone and temperature lidar validations performed within the framework of the Network for the Detection of Stratospheric Change, *J. Environ. Monit.*, *6*, 721–733.

Kerridge, B. J. K., R. Siddans, B. L. Latter, J. P. Burrows, M. Weber, R. De Beek, I. Aben, and W. Hartman (2003), GOME-2 error assessment study: Phase V extension, *Final Rep. EUM/CO/01/901/DK*, Eur. Organ. for the Exploit. of Meteorol. Satell., Darmstadt, Germany.

Khattatov, B. V., J.-F. Lamarque, L. V. Lyjak, R. Menard, P. Levelt, X. X. Tie, G. P. Brasseur, and J. C. Gille (2000), Assimilation of satellite observations of long-lived chemical species in global chemistry transport models, *J. Geophys. Res.*, *105*, 29,135–29,144.

Koelemeijer, R. B. A., P. Stammes, J. W. Hovenier, and J. F. de Haan (2001), A fast method for retrieval of cloud parameters using oxygen a band measurements from the Global Ozone Monitoring Experiment, *J. Geophys. Res.*, *106*, 3475–3490.

Kozlov, V. (1983), Design of experiments related to the inverse problem of mathematical physics (in Russian), in *Mathematical Theory of Experiment Design*, edited by C. M. Ermakov, pp. 216–246, Nauka, Moscow.

Kurosu, T. P., K. Chance, and R. J. D. Spurr (1999), CRAG—Cloud retrieval algorithm for ESA's GOME, in *Proceedings of the European Symposium on Atmospheric Measurements from Space (ESAMS-'99)*, pp. 513–521, Eur. Space Agency, Eur. Space Res. and Technol. Centre, Noordwijk, Netherlands.

Landgraf, J., O. P. Hasekamp, M. A. Box, and T. Trautmann (2001), A linearized radiative transfer model for ozone profile retrieval using the analytical forward-adjoint perturbation theory approach, *J. Geophys. Res.*, *106*, 27,291–27,306.

Landgraf, J., O. Hasekamp, R. van Deelen, and I. Aben (2004), Rotational Raman scattering of polarized light in the Earth atmosphere: A vector radiative transfer model using the radiative transfer perturbation theory approach, *J. Quant. Spectrosc. Radiat. Transfer*, *87*, 399–433.

Lumpe, J. D., R. M. Bevilacqua, K. W. Hoppel, and C. E. Randall (2002), POAM III retrieval algorithm and error analysis, *J. Geophys. Res.*, *107*(D21), 4575, doi:10.1029/2002JD002137.

Malicet, J., D. Daumont, D. J. Charbonnier, C. Parisse, A. Chakir, and J. Brion (1995), Ozone UV spetroscopy. II. Absorption cross-sections and temperature dependence, *J. Atmos. Chem.*, *21*, 263–273.

Martin, R. V., D. J. Jacob, K. Chance, T. P. Kurosu, P. I. Palmer, and M. J. Evans (2003), Global inventory of nitrogen oxide emissions constrained by space-based observations of NO_2 columns, *J. Geophys. Res.*, *108*(D17), 4537, doi:10.1029/2003JD003453.

McDermid, I. S., S. M. Godin, and T. D. Walsh (1990), Lidar measurements of stratospheric ozone and intercomparisons and validation, *Appl. Opt.*, *29*, 4914–4923.

McDermid, I. S., et al. (1998a), OPAL: Network for the Detection of Stratospheric Change Ozone Profiler Assessment at Lauder, New Zealand: 1. Blind intercomparison, *J. Geophys. Res.*, *103*, 28,683–28,692.

McDermid, I. S., et al. (1998b), OPAL: Network for the Detection of Stratospheric Change Ozone Profiler Assessment at Lauder, New Zealand: 2. Intercomparison of revised results, *J. Geophys. Res.*, *103*, 28,693–28,699.

McPeters, R. D. (1989), Climatology of nitric oxide in the upper stratosphere, mesosphere, and thermosphere: 1979 through 1986, *J. Geophys. Res.*, *94*, 3461–3472.

McPeters, R. D., et al. (1999), Results from the 1995 stratospheric ozone profile intercomparison at Mauna Loa, *J. Geophys. Res.*, *104*, 30,505–30,514.

McPeters, R. D., J. A. Logan, and G. J. Labow (2003), Ozone climatological profiles for Version 8 TOMS and SBUV retrievals, *Eos Trans. AGU*, *84*(46), Fall Meet. Suppl., Abstract A21D-0998.

Measures, R. M. (1984), *Laser Remote Sensing*, John Wiley, Hoboken, N. J.

Meijer, Y. J., R. J. van der A, R. F. van Oss, D. P. J. Swart, H. M. Kelder, and P. V. Johnston (2003), Global Ozone Monitoring Experiment ozone profile characterization using interpretation tools and lidar measurements for intercomparison, *J. Geophys. Res.*, *108*(D23), 4723, doi:10.1029/2003JD003498.

Meijer, Y. J., et al. (2004), Pole-to-pole validation of Envisat GOMOS ozone profiles using data from ground-based and balloon sonde measurements, *J. Geophys. Res.*, *109*, D23305, doi:10.1029/2004JD004834.

Müller, M. (1993), A scaled conjugate gradient algorithm for fast supervised learning, *Neural Networks*, *6*, 525–533.

Müller, M. D. (2002), Bestimmung von atmosphärischem Gesamtozon und Ozonprofilen aus GOME Daten mit Hilfe des Neural Network Ozone Retrieval System (NNORSY) (in German), Ph.D. thesis, Inst. of Environ. Phys. Univ. Bremen, Germany.

Müller, M. D., A. K. Kaifel, M. Weber, S. Tellmann, J. P. Burrows, and D. Loyola (2003), Ozone profile retrieval from Global Ozone Monitoring Experiment (GOME) data using a neural network approach (Neural Network Ozone Retrieval System (NNORSY)), *J. Geophys. Res.*, *108*(D16), 4497, doi:10.1029/2002JD002784.

Munro, R., R. Siddans, W. J. Reburn, and B. J. K. Kerridge (1998), Direct measurement of tropospheric ozone distributions from space, *Nature*, *392*, 168–171.

Network for the Detection of Stratospheric Change (1986), Report of the workshop in Boulder, ColoradoReport of the workshop in Boulder, Colorado, March 5–7, 1986, *Rep. EE*, Upper Atmos. Res. Prog., Washington, D. C.

Orphal, J. (2003), A critical review of the absorption cross-sections of O_3 and NO_2 in the 240–790 nm region, *J. Photochem. Photobiol. A*, *157*, 185–209.

Paur, R. J., and A. M. Bass (1984), The ultraviolet cross-sections of ozone: II. Results and temperature dependence, in *Proceedings of the Quadrennial Ozone Symposium*, pp. 611–616, Springer, New York.

Phillips, D. L. (1962), A technique for the numerical solution of certain integral equations of the first kind, *J. Assoc. Comput. Math.*, *9*, 84–97.

Riedmiller, M. (1994), Rprop—Description and implementation details, technical report, Inst. für Logik, Komplexität und Deduktionssysteme Univ. Karlsruhe, Germany.

Riishøjgaard, L. P. (1998), A direct way of specifying flow-dependent background error correlations for meteorological analysis systems, *Tellus, Ser. A*, *50*, 42–57.

Rodgers, C. D. (1990), Characterization and error analysis of profiles retrieved from remote sounding measurements, *J. Geophys. Res.*, *95*, 5587–5595.

Rodgers, C. D. (2000), *Inverse Methods for Atmospheric Sounding: Theory and Practice*, Ser. Atmos. Oceanic Planet. Phys., vol. 2, World Sci., Hackensack, N. J.

Rose, K., and G. Brasseur (1989), A three-dimensional model of chemically active trace species in the middle atmosphere during disturbed winter conditions, *J. Geophys. Res.*, *94*, 16,387–16,403.

Rozanov, V. V., D. Diebel, R. J. D. Spurr, and J. P. Burrows (1997), GOMETRAN: A radiative transfer model for the satellite project GOME, the plane-parallel version, *J. Geophys. Res.*, *102*, 16,683–16,695.

Rozanov, V. V., T. Kurosu, and J. P. Burrows (1998), Retrieval of atmospheric constituents in the UV-visible: A new quasi-analytical approach for the calculation of weighting functions, *J. Quant. Spectrosc. Radiat. Transfer*, *60*, 277–299.

Rumelhart, D. E., G. Hinton, and R. Williams (1986), Learning internal representations by error backpropagation, in *Parallel Distributed Processing*, vol. 1, pp. 318–362, MIT Press, Cambridge, Mass.

Russell, J. M., III, L. L. Gordley, J. H. Park, S. R. Drayson, W. D. Hesketh, R. J. Cicerone, A. F. Tuck, J. E. Frederick, J. E. Harries, and P. J. Crutzen (1993), The Halogen Occultation Experiment, *J. Geophys. Res.*, *98*, 10,777–10,797.

Schutgens, N. A. J., and P. Stammes (2003), A novel approach to the polarization correction of spaceborne spectrometers, *J. Geophys. Res.*, *108*(D7), 4229, doi:10.1029/2002JD002736.

Siddans, R. (2002), Height resolved ozone retrievals from GOME, Ph.D. thesis, Univ. of Reading, Reading, U. K.

Sioris, C. E., and W. F. J. Evans (2000), Impact of rotational Raman scattering in the O_2A band, *Geophys. Res. Lett.*, *27*, 4085–4088.

Spurr, R. J. D., T. P. Kurosu, and K. V. Chance (2001), A linearized discrete ordinate radiative transfer model for atmospheric remote sensing retrieval, *J. Quant. Spectrosc. Radiat. Transfer*, *68*, 689–735.

Swinbank, R., and A. O'Neill (1994), A stratosphere-troposphere data assimilation system, *Mon. Weather Rev.*, *122*, 686–702.

Tellmann, S., V. V. Rozanov, M. Weber, and J. P. Burrows (2004), Improvements in the tropical ozone profile retrieval from GOME UV/vis nadir spectra, *Adv. Space Res.*, *34*, 739–743.

Thomas, W., F. Baier, T. Erbertseder, and M. Kästner (2003), The Algeria severe weather event of November 1999 and its impact on ozone and NO_2 distributions, *Tellus, Ser. B*, *55*, 993–1006.

Thompson, A. M., et al. (2003), Southern Hemisphere Additional Ozonesondes (SHADOZ) 1998–2000 tropical ozone climatology: 1. Comparison with Total Ozone Mapping Spectrometer (TOMS) and ground-based measurements, *J. Geophys. Res.*, *108*(D2), 8238, doi:10.1029/2001JD000967.

Tikhonov, A. N. (1963), On the solution of incorrectly stated problems and a method of regularization, *Dokl. Akad. Nauk SSSR*, *151*, 501–504.

van der A, R. J., R. F. van Oss, A. J. M. Piters, J. P. F. Fortuin, Y. J. Meijer, and H. M. Kelder (2002), Ozone profile retrieval from recalibrated Global Ozone Monitoring Experiment data, *J. Geophys. Res.*, *107*(D15), 4239, doi:10.1029/2001JD000696.

van Geffen, J. H. G. M. (2004), Wavelength calibration of spectra measured by the Global Ozone Monitoring Experiment: Variations along orbits and in time, *Appl. Opt.*, *43*, 695–706.

van Geffen, J. H. G. M., and R. F. van Oss (2003), Wavelength calibration of spectra measured by GOME using a high-resolution reference spectrum, *Appl. Opt.*, *42*, 2739–2753.

van Oss, R. F., and R. J. D. Spurr (2002), Fast and accurate 4 and 6 stream linearised discrete ordinate radiative transfer models for ozone profile remote sensing retrieval, *J. Quant. Spectrosc. Radiat. Transfer*, *75*, 177–220.

Veiga, R. E., D. M. Cunnold, W. P. Chu, and M. P. McCormick (1995), Stratospheric aerosol and gas experiments I and II comparisons with ozonesondes, *J. Geophys. Res.*, *100*, 9073–9090.

Voigt, S., J. Orphal, and J. P. Burrows (1999), UV-visible absorption cross-sections of NO_2 and O_3 at atmospheric temperatures and pressures by FTS, in *Proceedings of the European Symposium on Atmospheric Measurements from Space (ESAMS-'99)*, pp. 471–475, Eur. Space Agency, Eur. Space Res. and Technol. Centre, Noordwijk, Netherlands.

Wang, H. J., D. M. Cunnold, L. W. Thomason, J. M. Zawodny, and G. E. Bodeker (2002), Assessment of SAGE version 6.1 ozone data quality, *J. Geophys. Res.*, *107*(D23), 4691, doi:10.1029/2002JD002418.

Zehner, C., and S. Casadio (2000), Temperature independent differential absorption spectroscopy (TIDAS) for the measurement of ozone slant content using GOME data, paper presented at the Quadriennial Ozone Symposium, Int. Assoc. for Meteorol. and Atmos. Sci., Sapporo, Japan.

————————
F. Baier and T. Erbertseder, German Aerospace Center, German Remote Sensing Data Center, DFD, D-82234 Wessling, Germany. (frank.baier@dlr.de; thilo.erbertseder@dlr.de)

P. K. Bhartia, NASA Goddard Space Flight Center, Code 916/Code 613.3, Greenbelt, MD 20904, USA. (bhartia@carioca.gsfc.nasa.gov)

G. E. Bodeker, NIWA, Private Bag 50061, Omakau, Central Otago, Lauder, 9182, New Zealand. (g.bodeker@niwa.co.nz)

S. Casadio, SERCO spa, Frascati, Italy. (stefano.casadio@esa.int)

K. Chance and X. Liu, Harvard-Smithsonian Center for Astrophysics, 60 Garden Street, Cambridge, MA 02138-1516, USA. (kchance@cfa.harvard.edu;xliu@cfa.harvard.edu)

F. Del Frate, Dipartimento di Informatica Sistemi e Produzione, Tor Vergata University, Via del Politecnico 1, I-00133, Rome, Italy. (delfrate@disp.uniroma2.it)

M. D. Felder, Leibniz Computing Centre, Bolzmannstrasse 1, D-85748 Garching, Germany. (felder@lrz.de)

L. E. Flynn, NOAA/NESDIS, 5200 Auth Road, Camp Springs, MD 20746-4304, USA. (lawrence.e.flynn@noaa.gov)

S. Godin-Beekmann, Service d'Aeronomie du CNRS, Universite Pierre et Marie Curie, 4, Place Jussieu, F-75252 Paris Cedex 05, France. (sophie.godin@aero.jussieu.fr)

G. Hansen, Polar Environmental Centre, Norwegian Institute for Air Research, N-9296 Tromsø, Norway. (ghh@nilu.no)

O. P. Hasekamp and J. Landgraf, Space Research Organization Netherlands, Sorbonnelaan 2, NL-3584 CA Utrecht, Netherlands. (o.p.hasekamp@sron.nl; j.landgraf@sron.nl)

A. Kaifel, Center for Solar Energy and Hydrogen Research, Hessbruhlstr. 21c, D-70565 Stuttgart, Germany. (anton.kaifel@zsw-bw.de)

H. M. Kelder, R. J. van der A, and R. F. van Oss, KNMI, PO Box 201, 3730 AE B-De Bilt, Netherlands. (kelder@knmi.nl; avander@knmi.nl; ossvanr@knmi.nl)

B. J. Kerridge, B. Latter, and R. Siddans, Rutherford Appleton Laboratory, Chilton, Didcot, OX11 0QX UK. (b.j.kerridge@rl.ac.uk; b.g.latter@rl.ac.uk; r.siddans@rl.ac.uk)

J.-C. Lambert, Space Aeronomy Institute of Belgium, 3, Avenue Circulaire, B-1180 Brussels, Belgium. (lambert@bira-iasb.oma.be)

I. S. McDermid, Jet Propulsion Laboratory, Table Mountain Facility, P.O. Box 367, 2440 Table Mountain Road, Wrightwood, CA 92397, USA. (mcdermid@tmf.jpl.nasa.gov)

Y. J. Meijer and D. P. J. Swart, LVM, Environmental Risks and Safety Division, RIVM, P.O. Box 1, 3720 BA Bilthoven, Netherlands. (yasjka.meijer@rivm.nl; daan.swart@rivm.nl)

Y. Pachepsky, STG, Inc., 11710 Plaza America Dr, Suite 1200, Reston, VA 20190, USA. (yakov.pachepsky@noaa.gov)

V. Rozanov, S. Tellmann, and M. Weber, Institute of Environmental Physics, University of Bremen, P.O. Box 330440, D-28334 Bremen, Germany. (rozanov@iup.physik.uni-bremen.de; tellmann@iup.physik.uni-bremen.de; weber@iup.physik.uni-bremen.de)

C. Zehner, ESA/ESRIN, Via Galilieo Galileo C.P. 64, I-00044 Frascati, Italy. (claus.zehner@esa.int)